

Extreme Geomagnetic Storms – 1868 – 2010

S. Vennerstrom¹ · L. Lefevre² · M. Dumbović³ ·
N. Crosby⁴ · O. Malandraki⁵ · I. Patsou⁵ · F. Clette² ·
A. Veronig⁶ · B. Vršnak³ · K. Leer¹ · T. Moretto⁷

Received: 4 September 2015 / Accepted: 25 April 2016 / Published online: 19 May 2016
© Springer Science+Business Media Dordrecht 2016

Abstract We present the first large statistical study of extreme geomagnetic storms based on historical data from the time period 1868–2010. This article is the first of two companion papers. Here we describe how the storms were selected and focus on their near-Earth characteristics. The second article presents our investigation of the corresponding solar events and their characteristics. The storms were selected based on their intensity in the aa index, which constitutes the longest existing continuous series of geomagnetic activity. They are analyzed statistically in the context of more well-known geomagnetic indices, such as the Kp and Dcx/Dst index. This reveals that neither Kp nor Dcx/Dst provide a comprehensive geomagnetic measure of the extreme storms. We rank the storms by including long series of single magnetic observatory data. The top storms on the rank list are the New York Railroad storm occurring in May 1921 and the Quebec storm from March 1989. We identify key characteristics of the storms by combining several different available data sources, lists of storm sudden commencements (SSCs) signifying occurrence of interplanetary shocks, solar wind *in-situ* measurements, neutron monitor data, and associated identifications of Forbush decreases as well as satellite measurements of energetic proton fluxes in the near-Earth space environment. From this we find, among other results, that the extreme storms are very strongly correlated with the occurrence of interplanetary shocks (91–100 %), Forbush decreases (100 %), and energetic solar proton events (70 %). A quantitative comparison of these associations relative to less intense storms is also presented. Most notably, we find that most often the extreme storms are characterized by a complexity that is associated with

✉ S. Vennerstrom
sv@space.dtu.dk

¹ National Space Institute, DTU Space, Elektrovej B327, 2800 Kgs. Lyngby, Denmark

² Royal Observatory of Belgium, Brussels, Belgium

³ Hvar Observatory, Faculty of Geodesy, University of Zagreb, Zagreb, Croatia

⁴ Royal Belgian Institute for Space Aeronomy, Brussels, Belgium

⁵ IAASARS, National Observatory of Athens, Athens, Greece

⁶ University of Graz, Graz, Austria

⁷ National Science Foundation, Arlington, USA

multiple, often interacting, solar wind disturbances and that they frequently occur when the geomagnetic activity is already elevated. We also investigate the semiannual variation in storm occurrence and confirm previous findings that geomagnetic storms tend to occur less frequently near solstices and that this tendency increases with storm intensity. However, we find that the semiannual variation depends on both the solar wind source and the storm level. Storms associated with weak SSC do not show any semiannual variation, in contrast to weak storms without SSC.

Keywords Geomagnetic storms · Extreme events · Historic data

1. Introduction

Geomagnetic storms are an increasing societal concern, in particular the most intense storms and their possible effects on power grids, satellites, and communications. In response, significant effort has been devoted to investigating very intense geomagnetic storms and their causes (Tsurutani *et al.*, 1992; Bell, Gussenhoven, and Mullen, 1997; Richardson *et al.*, 2006; Gonzalez *et al.*, 2007, 2011b; Zhang *et al.*, 2007; Echer, Gonzales, and Tsurutani, 2008; Tsurutani and Lakhina, 2013). A major obstacle in these investigations is the fact that very intense storms occur infrequently, and only few examples exist during the most recent solar cycles. To enlarge the statistical basis, we present here a study of the most intense storms that have occurred since 1868 as observed in the longest existing continuous series of geomagnetic activity, the aa index.

Most previous studies of intense storms are based on the Dst and not on the aa index. Storms are typically selected and classified as moderate, intense, or super intense, depending on their peak Dst value. Although the Dst is traditionally considered as the primary index for measuring geomagnetic storms, it is by no means adequate to quantify all of the space weather effects associated with geomagnetic storms. For example the magnetospheric ring current, which is the primary source for the Dst decrease during storms, is not an important source for geomagnetically induced currents (GICs) that influence power grids or for ionospheric disturbances that influence communication and navigation. For these effects high- and mid-latitude magnetic indices such as the AE, Kp, ap, and aa indices provide much more direct measures of the inducing geomagnetic disturbances. In particular, the intensification of the auroral electrojets and their equatorward migration during magnetic storms are an important source of GICs because of the associated fast magnetic variations. This is reflected in the method used for storm classification in the space weather community. Here the most widely used index is the Kp index, which forms the basis for the NOAA “G”-scale of storms (<http://www.swpc.noaa.gov/noaa-scales-explanation>), for example.

Strong storms are well known to be primarily associated with the passage of fast interplanetary coronal mass ejections (ICMEs) (*e.g.* Gosling *et al.*, 1990; Gonzalez *et al.*, 2007), primarily because fast ICMEs are associated with high solar wind speeds and often with strong southward interplanetary magnetic field IMF. These conditions drive enhanced reconnection with the magnetospheric field (Dungey, 1961), leading to intense substorm activity and ring current build-up. In a recent study, Richardson and Cane (2011a, 2011b) investigated the statistical relation between solar wind parameters observed in association with ICMEs and the resulting geomagnetic effect in the indices Dst and Kp. They found a high linear correlation between the coupling function vB_s and the storm peak magnitude. Here v denotes the solar wind speed and B_s the southward component of the IMF. The correlation coefficient was close to 0.9 both for Kp and Dst (Richardson and Cane 2011a, 2011b). These

results together with the similar classification terms used in Kp-based and Dst-based storm classification might suggest that the Kp-based and Dst-based storm classification leads to similar results. As we show below, however, this may be far from true, in particular for the extreme storms.

In the work presented here we investigate the strongest geomagnetic storms observed in the aa index by statistically combining the available relevant data for these events including a wide variety of observations in the chain of events from the Sun to Earth. This includes information on sunspots, solar flares, solar energetic particles, galactic cosmic-ray variations, solar wind, and geomagnetic activity. The results are presented in two companion articles. This first article focuses on identifying the storms and describing the storm characteristics. Specifically, near-Earth observations are analyzed to determine the reason for the storms intensity. We also analyze the storm characteristics statistically in comparison with less intense storms. In the second article (Léfevre *et al.*, 2016), we investigate the possible solar sources of these storms and their characteristics in order to determine which occurrences at the Sun led to these events.

2. Data and Method

2.1. Data Sources

Near-Earth observations including a variety of geomagnetic parameters, *in-situ* solar wind parameters, cosmic-ray intensity measurements, and some solar energetic particle characteristics are used in this study. They are presented below.

2.1.1. Geomagnetic Data

The starting point of the investigation is the aa index that is provided by the International Service of Geomagnetic Indices (<http://isgi.unistra.fr/>). This is a three-hour range index derived similarly to the ap (and hence Kp) index, but based on K-values from only two stations that are approximately antipodal. Using this series, we have developed an algorithm for the automatic identification of geomagnetic storm periods and calculation of various derived parameters, as we describe below. The storms defined in this way are analyzed in context with other well-known indices, such as the Kp index (1932–present) provided by the GeoforschungsZentrum (GFZ) in Potsdam (http://www-app3.gfz-potsdam.de/kp_index/index.html), the Dst index (1957–present) provided by WDCC2 for Geomagnetism in Kyoto (<http://wdc.kugi.kyoto-u.ac.jp>), and the Dcx index (1932–present), which was newly designed and made available by the University of Oulu (<http://dcx.oulu.fi>).

The aa index was chosen as the basis for this study because it is the longest existing continuous measure of geomagnetic activity, having been derived continuously since 1868. No other current index is available back to the end of the nineteenth century. However, because the index is based on only two stations, we supplemented the aa series with a number of long geomagnetic data series from single observatories. These series consist of hourly values of either the three vector components X, Y, and Z or equivalently the three magnetic elements, horizontal component (H), declination (D), and vertical component (Z).

Specifically, we used nine long series of observatory data, some of which consist of data from two or three consecutive observatories. Typically in these cases an observatory was moved to a place close by and given a new name. For the purpose of this analysis we consider this a single observatory series. Table 1 lists the observatories. The first column

Table 1 Geomagnetic observatories with long data series used as supplement to determine the relative storm intensity, location of observatory, IAGA code of observatory, start and end years of data series, geographic latitude and longitude, and corrected geomagnetic (cgm) latitude and longitude.

Location	IAGA	Year start	Year end	geolat	geolon	cgm-lat	cgm-lon
Hawaii	HON	1902	2010	21.32	202.00	21.40	269.82
Japan	TOK	1897	1912	35.69	139.75	28.73	211.35
	KAK	1913	2010	36.23	140.19	29.28	211.77
Puerto Rico	VQS	1903	1965	18.15	294.55	NaN	NaN
	SJG	1926	2010	18.12	293.85	NaN	NaN
Washington	CLH	1901	1956	38.73	283.16	49.62	358.59
	FRD	1956	2010	38.21	282.63	49.16	357.79
France	PSM	1883	1900	48.81	2.49	44.41	79.75
	VLJ	1901	1936	48.82	2.02	44.44	79.37
	CLF	1936	2010	48.02	2.27	43.43	79.35
Germany	NGK	1890	2010	52.07	12.68	47.95	89.17
Netherlands	DBN	1903	1938	52.10	5.18	48.27	82.95
	WIT	1938	1984	52.81	6.67	49.04	84.81
Russia	EKT	1887	1925	56.83	60.63	52.71	133.84
	SVD	1930	1980	56.73	61.07	52.61	134.25
	ARS	1973	2010	56.43	58.57	52.32	131.81
Alaska	SIT	1902	2010	57.07	224.67	59.75	280.05

lists the nine regions where the observatories, or sets of observatories, are located. The second column shows the three-letter IAGA code of each individual observatory, which was changed when the observatory was moved. The next two columns show the start and end years of the data series from each observatory. The last columns provide the geographical latitude and longitude as well as the corrected geomagnetic coordinates in 2000, computed using the International Geomagnetic Reference Field model. The table shows that three low-latitude data series, five mid-latitude data series, and one sub-auroral data series are included.

In addition to the geomagnetic indices and observatory data, lists of geomagnetic storm sudden commencements (SSCs) were used. To obtain SSC information for the entire period from 1868 to the present, several consecutive lists of SSCs based on a varying number of stations were included. The longest, and therefore the primary, list has been compiled by Mayaud (1973). This list covers the period 1868–1967. It is based on one or two equatorial stations, but mid-latitude stations from both hemispheres are also included. This list was extended in time for several periods based on extended sets of stations: 1968–1975 (IAGA Bulletin No. 39), 1976–1982 (IAGA Bulletins No. 32g-m), and Preliminary Reports of the ISGI (DeBilt, 1981–1987; Institute de Physique du Globe, France, 1988–1989). From 1990 to the present the series was supplemented by the NGDC SSC list for 1968 to the present (which does not include the SSC amplitudes).

2.1.2. Solar Wind Data

The *in-situ* solar wind observations used in the study are from the so-called OMNI database of hourly values of solar wind plasma and magnetic field parameters made available by the Goddard Space Flight Center (GSFC) Space Physics Data Facility (SPDF) (<http://omniweb.gsfc.nasa.gov>). Data are available for 1967 to the present.

2.1.3. Neutron Monitor Data

To investigate the occurrence of Forbush decreases, the hourly averaged count rates from nine neutron monitor (NM) stations, corrected for atmospheric pressure, were used. The stations included and the corresponding rigidities are as follows: Yakutyk (1.70 GV), Churchill (0.21 GV), Uppsala (1.43 GV), Moscow (2.43 GV), Kiel (2.29 GV), Irkutsk (3.66 GV), Goose bay (0.52 GV), Calgary (1.09 GV), and Novosibirsk (2.80 GV). These data were obtained from the SPIDR website (<http://spidr.ngdc.noaa.gov/spidr/>), and cover the period from 1957 to the present.

2.1.4. Solar Energetic Particle Data

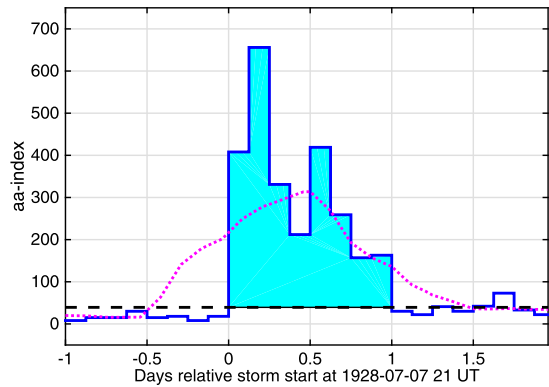
For this study the ESA Solar Energetic Particle Environment Modelling (SEPEM) reference proton dataset (Crosby *et al.* (2015); <http://dev.sepem.oma.be>), consisting of energetic proton data in the energy range of 5–200 MeV, was used. The dataset is built on proton data (5-min averaged intensities) measured by near-Earth spacecraft (GOES, IMP8) and extends back to November 1973.

The FP7 COMESEP SSE list was used (Dierckxsens *et al.*, 2015), which is a subset of the ESA SEPEM reference proton event list, called the SEPEM sub-event (SSE) list. This is based on the proton energy range 7.23–10.45 MeV (Crosby *et al.*, 2015). The majority of events in the SEPEM list have a clear counterpart in a subset of the Cane, Richardson, and von Rosenvinge SEP list (CRR2010 list, Cane, Richardson, and Rosenvinge, 2010). In some cases, SEPEM events are the sum of several individual SEP events because a dwell time of at least 24 hours is required between consecutive events. When the COMESEP SSE list was built, these SEPEM events were therefore split up into separate events based on the start times of events in the CRR2010 list. The COMESEP SSE list covers the SOHO era (1997–2006) and is comprised of 90 SEP events.

2.2. Storm Identification and Derivation of Storm Parameters

The storm periods were identified based on the aa index using the following procedure. First, individual aa values higher than a given storm peak limit were identified. For the extreme storms investigated in our articles, we chose an aa limit higher than or equal to 300, which results in a total of 105 storms. For each of the individual values exceeding 300 the beginning of that particular storm period was defined as the hour where aa exceeds 40 and the end of that storm as the end time of the last aa value exceeding 40 (see Figure 1). The threshold value of 40 was chosen because it corresponds to twice the value of the average of aa for the entire dataset ($2 \cdot \langle aa \rangle$). The procedure is illustrated in Figure 1. When the storm period (start and end times) was defined, various derived parameters were determined, including

Figure 1 Illustration of the definition of storm periods and some associated storm parameters. The solid (blue) curve is the aa index and the shaded area shows the storm period. The black dashed line shows the used threshold $aa = 40$, and the dotted (magenta) curve is the 24-hour running mean of the aa index.



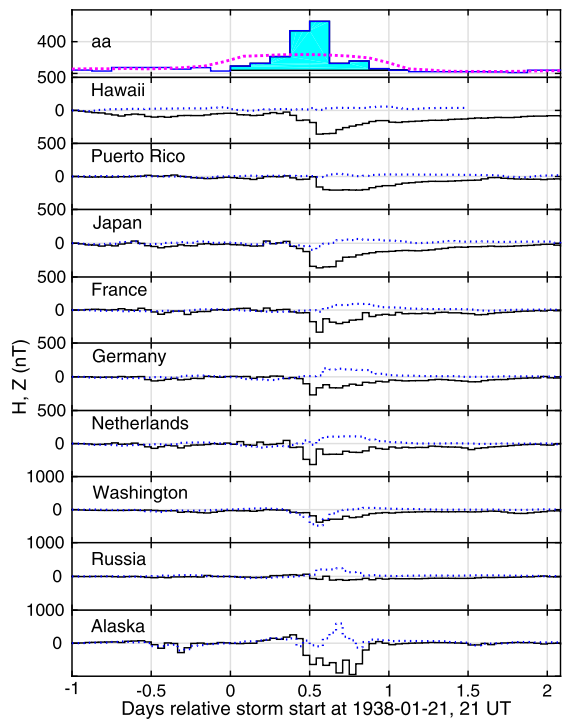
the peak aa-value, the time of the maximum, and the number of individual peaks (two in the example of Figure 1).

2.3. Single Observatory Data and Ranking of the Storms

To further characterize the magnetic storms, we used the horizontal (H) and vertical (Z) components of nine magnetic observatories as described in Section 2.1. During each storm period as defined by the aa index, the absolute value of the range in H and Z was computed at each observatory. The effect of the regular “quiet day” diurnal variation, which is normally subtracted when deriving mid-latitude indices, was ignored here because it was negligible compared to the large range values observed during extreme geomagnetic storms. In addition to the aa index, these ranges then constitute 18 additional parameters that contribute to the description of the storm intensity. Figure 2 shows the hourly value H and Z variations for the nine selected stations during one of the storm periods occurring in 1938. The top panel shows the aa index and the defined storm period over which the range is computed. The following panels display the disturbance in the H (solid black) and Z (dotted blue) components at the nine observatories ordered by magnetic latitude with the lowest magnetic latitude at the top. We note that the scale changes for the bottom three panels.

The magnetic variations are strongly latitude dependent, therefore we normalized the range parameters to combine or compare information from stations at different latitudes. We did this for each range parameter (H and Z components, respectively, for each station) by dividing with the average over all storms for that parameter. The normalized parameters were then combined in different ways to describe the storm intensity in more detail. Specifically, we computed individual measures for storm intensity at low- and mid-latitudes by averaging the normalized parameters for the low- and mid-latitude stations, respectively. For the aa index, storm peak values were computed and likewise normalized by dividing with the average over all the storms. In addition, the storm-peak values for the 24-hour running means of aa (purple curve in Figures 1 and 2) were normalized in the same way. We also computed a measure combining all observatories and the aa index. For each storm, this ranking parameter was computed as the average over all of these normalized parameters, giving double weight to the aa-index parameters because they are based on two stations. When data gaps existed in any of the data series, the ranking parameter was computed from the remaining parameters. The existence of these data gaps is an important reason for including both the H and the Z component in the calculation.

Figure 2 Example of magnetic field variations recorded at geomagnetic observatories during an intense storm. For each observatory the variations in the H-component are displayed as a solid line and the Z-component as a dotted line. The top of the figure shows the aa index and the storm period in the same way as Figure 1.



With this we have a detailed measure of the relative intensity of the storms, either overall, or in a specific latitude range that allows us to rank the storms according to intensity in several ways. The measures of storm intensity using either mid-latitude observatories, low-latitude observatories, or the aa index alone are provided in Table 2. This table lists all 105 storms and several of the derived parameters characterizing the storms. In addition we listed the numbered ranking according to the overall ranking parameter that combines the aa and all the single observatory series together (last column). In this numbered ranking “Rank = 1” corresponds to the strongest event in the list. It is important to note that this ranking is not absolute and should only be taken as guidance in identifying the most intense storms. The ranking, of course, depends on the specific choice of stations and the ranking method used. Other parameters such as the storm duration could also have been included and might have produced different results. It should also be noted that the single observatory data are not available throughout the entire aa period. For the first 12 storms on the list that occurred during 1868–1882, only the aa index is available. For this reason we chose to also provide a ranking based only on the two aa parameters, namely the peak of aa and the peak of the 24-hour running means of aa. This ranking is included in the table as “aa rank”.

Nevanlinna and Kataja (1993) derived a backward extension of the aa index based on hourly observations of the magnetic declination in the subauroral station Helsinki. Based on monthly values, they found a correlation with the aa index of 0.96. The index was derived for the period 1844–1880. With an overlap with the aa index from 1868–1880, this could provide an interesting opportunity for a future study of the possibility of extending the extreme storm list further back in time.

Table 2 List of geomagnetic parameters for the 105 extreme storms; chronological storm number n , storm start time in the format YYYY-MM-DD HH:MM, time difference between storm start and storm peak in hours h_{peak} , storm duration in hours T_{storm} , aa peak value, aa index 24-hour running average peak value, Dcx index peak value, number of peaks in storm interval n_{peak} , number of associated SSCs n_{ssc} , time of SSC occurrence, aa index ranking measure aa_{rel} , mid-latitude observatories ranking measure mid_{rel} , low-latitude observatories ranking measure low_{rel} , rank based on aa index, overall or total rank based on aa index and all observatories.

n	Storm start time yyyy-mm-dd hh:mm	h_{peak}	T_{storm}	aa peak	aa24 peak	Dcx peak	n_{peak}	n_{ssc}	T_{ssc}	aa_{rel}	mid_{rel}	low_{rel}	aa rank	Total rank
1	1869-05-13 12:00	6	15	531	178		1	0	–	1.02	–	–	39	44
2	1870-09-24 03:00	12	54	334	216		5	1	09-24 02:36	0.89	–	–	55	61
3	1870-10-24 09:00	9	21	337	189		3	1	10-24 09:54	0.82	–	–	68	69
4	1870-10-25 09:00	6	18	464	185		1	1	10-25 12:12	0.96	–	–	48	49
5	1871-02-11 12:00	33	42	334	157		3	1	02-12 19:06	0.75	–	–	86	81
6	1871-04-09 15:00	6	30	337	121		3	1	04-09 16:36	0.66	–	–	97	91
7	1872-10-14 21:00	0	45	456	220		5	1	10-14 22:18	1.03	–	–	36	40
8	1880-08-12 09:00	3	48	334	142		4	1	08-12 11:36	0.71	–	–	93	85
9	1881-01-31 06:00	12	24	337	111		3	2	01-30 18:42	0.64	–	–	100	94
10	1882-04-16 21:00	15	24	536	289		2	1	04-16 23:12	1.29	–	–	24	20
11	1882-11-17 09:00	0	45	531	368		5	1	11-17 10:06	1.47	–	–	12	11
12	1882-11-19 12:00	21	39	536	296		2	0	–	1.3	–	–	21	17
13	1886-03-30 06:00	3	24	337	180		2	1	03-30 08:00	0.8	0.77	–	72	72
14	1892-02-13 03:00	21	39	658	263		3	2	02-13 23:48	1.36	1.18	–	17	22
15	1892-07-16 12:00	3	33	337	200		2	2	07-16 17:24	0.85	0.67	–	59	82
16	1892-08-12-12:00	6	18	536	160		1	2	08-12 17:48	0.98	0.61	–	43	80
17	1894-02-25 06:00	6	30	337	149		2	1	02-25 07:54	0.73	0.54	–	88	96
18	1894-07-20 06:00	6	21	531	225		2	1	07-20 06:06	1.13	1.31	–	33	25
19	1894-08-20 00:00	3	18	464	194		2	1	08-20 02:54	0.98	1.42	–	44	24
20	1898-03-15 00:00	21	33	334	162		3	2	03-15 00:48	0.76	0.73	0.6	83	84

Table 2 (Continued.)

<i>n</i>	Storm start time yyyy-mm-dd hh:mm	<i>h</i> _{peak}	<i>T</i> _{storm}	aa peak	aa24 peak	Dcx peak	<i>n</i> _{peak}	<i>n</i> _{ssc}	<i>T</i> _{ssc}	aa _{rel}	mid _{rel}	low _{rel}	aa rank	Total rank
21	1898-09-09 12:00	6	12	456	173		1	1	09-09 12:06	0.92	0.63	0.98	51	76
22	1903-10-31 03:00	9	30	658	314		2	1	10-31 06:00	1.48	1.97	1.4	10	6
23	1907-02-09 06:00	12	24	337	169		2	1	02-09 14:12	0.78	0.76	0.86	79	73
24	1908-09-11 15:00	6	24	410	174		1	3	09-11 21:48	0.87	1.03	1.26	57	38
25	1909-09-25 09:00	3	15	658	321		1	2	09-25 11:42	1.5	2.41	1.75	8	3
26	1915-06-17 00:00	15	27	337	194		2	2	06-17 01:48	0.84	0.85	0.91	61	62
27	1919-08-11 06:00	9	27	456	218		3	1	08-11 06:54	1.03	1.69	1.82	37	10
28	1920-03-22 09:00	15	45	346	237		5	1	03-22 09:06	0.95	1.32	1.7	50	18
29	1921-05-13 12:00	33	93	680	346		8	4	05-14 22:12	1.58	2.37	1.98	4	1
30	1926-01-26 15:00	9	15	338	148		2	1	01-26 16:18	0.73	0.65	0.76	90	86
31	1926-04-14 12:00	18	30	338	175		2	1	04-14 14:00	0.79	0.95	0.83	76	60
32	1926-10-14 00:00	42	57	448	219		3	2	10-15 07:36	1.02	0.94	0.86	38	54
33	1928-07-07 21:00	3	24	656	314		3	1	07-07 23:18	1.48	1.42	1.16	11	14
34	1938-01-21 21:00	12	27	656	238	-328	2	1	01-22 01:42	1.3	0.8	1.08	22	48
35	1938-01-25 09:00	9	21	656	233	-336	1	1	01-25 11:54	1.29	1.1	1.03	23	33
36	1938-04-16 03:00	3	21	656	174	-255	2	1	04-16 05:42	1.15	0.94	1.12	31	42
37	1938-05-11 15:00	3	36	331	163	-218	3	1	05-11 15:48	0.76	0.97	1.11	84	47
38	1939-04-24 15:00	3	33	408	143	-236	4	1	04-24 17:36	0.79	0.67	0.95	75	77
39	1940-03-24 06:00	9	51	526	369	-355	4	2	03-24 15:36	1.46	1.82	1.21	13	8
40	1940-03-29 09:00	48	84	331	209	-260	8	2	03-31 09:36	0.87	1.23	0.99	58	37
41	1940-06-25 00:00	12	27	331	134	-132	3	1	06-25 02:48	0.69	0.56	0.48	95	102
42	1941-03-01 03:00	12	24	656	246	-449	2	1	03-01 03:54	1.32	2.16	1.24	19	4

Table 2 (Continued.)

<i>n</i>	Storm start time yyyy-mm-dd hh:mm	<i>h</i> _{peak}	<i>T</i> _{storm}	aa peak	aa24 peak	Dcx peak	<i>n</i> _{peak}	<i>n</i> _{ssc}	<i>T</i> _{ssc}	aq _{rel}	mid _{rel}	low _{rel}	aa rank	Total rank
43	1941-07-04 18:00	18	33	526	292	-431	3	1	07-05 05:00	1.28	1.53	1.26	25	12
44	1941-09-18 03:00	12	51	526	422	-404	3	1	09-18 04:12	1.59	1.99	1.46	3	5
45	1942-03-01 06:00	0	24	331	162	-99	2	1	03-01 07:30	0.75	0.59	0.68	85	93
46	1944-12-15 21:00	18	24	331	121	-181	2	1	12-15 18:54	0.66	0.72	0.62	98	89
47	1946-02-07 06:00	3	39	408	255	-214	3	1	02-07 10:18	1.06	0.8	0.72	34	67
48	1946-03-24 21:00	15	39	331	190	-224	3	0	-	0.82	0.97	0.61	69	66
49	1946-03-28 03:00	9	36	656	318	-468	2	2	03-28 06:30	1.49	1.92	1.34	9	7
50	1946-07-26 18:00	0	21	331	193	-264	2	1	07-26 18:42	0.83	1.18	1.18	66	35
51	1946-09-22 03:00	6	48	656	290	-163	4	3	09-22 10:12	1.42	0.92	0.91	15	43
52	1947-08-22 06:00	3	15	338	109	-156	1	1	08-22 09:06	0.64	0.58	0.57	102	98
53	1948-10-17 21:00	0	12	338	111	-158	1	1	10-17 22:06	0.64	0.49	0.6	99	103
54	1949-01-24 18:00	24	51	338	196	-334	6	1	01-24 18:24	0.84	1.05	1.43	60	32
55	1949-05-12 06:00	9	24	448	200	-258	1	1	05-12 06:36	0.98	0.95	0.96	45	50
56	1951-10-28 09:00	9	15	331	114	-227	1	1	10-28 11:48	0.64	0.68	0.72	101	88
57	1957-01-21 06:00	15	30	490	186	-256	1	1	01-21 12:54	0.99	0.76	0.83	42	68
58	1957-03-01 12:00	15	45	357	152	-224	4	2	03-02 05:06	0.76	0.69	1.05	82	71
59	1957-09-04 12:00	3	42	434	205	-320	4	1	09-04 13:00	0.97	1.15	1.04	46	36
60	1957-09-13 00:00	9	18	357	157	-419	1	1	09-13 00:42	0.77	0.98	1.28	80	41
61	1957-09-29 03:00	12	39	357	142	-250	4	1	09-29 00:12	0.74	0.95	0.88	87	58
62	1958-02-10 15:00	9	45	568	292	-421	4	1	02-11 01:24	1.33	1.12	1.43	18	23
63	1958-07-08 06:00	9	36	698	305	-321	4	1	07-08 07:48	1.5	1.37	1.17	7	15
64	1958-09-04 12:00	3	21	357	180	-301	3	0	-	0.83	0.95	1	67	53

Table 2 (Continued.)

<i>n</i>	Storm start time yyyy-mm-dd hh:mm	<i>h</i> _{peak}	<i>T</i> _{storm}	aa peak	aa24 peak	Dcx peak	<i>n</i> _{peak}	<i>n</i> _{ssc}	<i>T</i> _{ssc}	aq _{rel}	mid _{rel}	low _{rel}	aa rank	Total rank
65	1959-03-26 06:00	33	42	357	173	-242	4	1	03-26 08:42	0.81	0.79	0.87	71	70
66	1959-05-11 21:00	18	27	302	117	-87	3	1	05-11 23:24	0.62	0.5	0.52	105	104
67	1959-07-15 06:00	9	24	698	344	-418	2	1	07-15 08:00	1.6	1.7	1.27	2	9
68	1959-07-17 15:00	3	27	355	183	-167	2	1	07-17 16:43	0.83	0.76	0.81	63	74
69	1960-03-31 03:00	36	60	490	307	-327	5	0	-	1.28	1.41	1.17	27	16
70	1960-04-29 00:00	39	63	568	209	-316	6	2	04-30 12:12	1.13	1.31	0.96	32	29
71	1960-10-05 21:00	24	54	357	250	-271	3	1	10-06 02:36	0.99	1.04	0.97	41	45
72	1960-11-12 12:00	18	48	568	369	-310	3	2	11-12 18:42	1.51	1.22	1	6	28
73	1960-11-15 12:00	12	30	357	161	-174	3	1	11-15 13:00	0.78	0.67	0.62	77	90
74	1961-07-27 03:00	6	24	357	131	-143	2	1	07-26 19:48	0.71	0.55	0.64	92	97
75	1961-10-28 06:00	12	30	357	170	-274	2	1	10-28 08:06	0.8	0.87	0.79	73	65
76	1963-09-21 12:00	33	42	357	182	-224	3	1	09-21 14:12	0.83	0.71	0.88	65	75
77	1967-02-16 06:00	3	15	355	95	-122	2	2	02-16 08:30	0.62	0.39	0.49	103	105
78	1967-05-25 09:00	12	30	568	272	-375	3	1	05-25 12:36	1.28	1.39	1.43	26	13
79	1969-02-02 15:00	3	33	434	118	-181	4	1	02-02 15:02	0.76	0.45	0.74	81	101
80	1970-03-07 12:00	30	42	568	178	-283	4	1	03-08 14:17	1.06	0.88	0.92	35	55
81	1972-08-04 12:00	9	57	698	284	-110	5	3	08-04 20:54	1.45	0.8	0.74	14	56
82	1981-07-25 03:00	9	39	357	174	-209	4	2	07-25 13:22	0.81	0.98	1	70	51
83	1982-07-13 03:00	18	69	490	263	-326	5	1	07-13 16:18	1.17	1.15	1.49	30	27
84	1982-09-05 21:00	15	51	434	202	-265	5	2	09-06 07:53	0.96	1.1	0.89	47	39
85	1986-02-07 09:00	33	63	578	280	-268	5	0	-	1.31	1.26	0.94	20	26
86	1989-03-13 00:00	21	69	715	431	-565	5	2	03-13 07:43	1.82	2.29	1.62	1	2

Table 2 (Continued.)

<i>n</i>	Storm start time yyyy-mm-dd hh:mm	<i>h</i> _{peak}	<i>T</i> _{storm}	aa peak	aa24 peak	Dcx peak	<i>n</i> _{peak}	<i>n</i> _{ssc}	<i>T</i> _{ssc}	aq _{rel}	mid _{rel}	low _{rel}	aa rank	Total rank
87	1989-10-20 06:00	12	66	306	184	-274	6	1	10-20 09:17	0.78	0.89	0.89	78	63
88	1989-11-17 06:00	12	27	363	197	-254	2	1	11-17 09:25	0.87	0.76	0.7	56	78
89	1991-03-24 03:00	0	27	363	181	-284	3	2	03-24 03:41	0.84	0.7	1.16	62	59
90	1991-06-04 12:00	27	48	363	208	-202	4	2	06-04 15:36	0.9	0.87	0.97	53	57
91	1991-11-08 06:00	15	42	578	231	-366	4	2	11-08 13:13	1.19	1.03	1.18	29	34
92	1992-09-09 00:00	9	51	310	115	-123	4	2	09-09 01:39	0.62	0.58	0.57	104	99
93	2000-04-06 15:00	6	18	363	167	-294	1	0	-	0.8	0.67	0.92	74	83
94	2000-07-15 03:00	12	36	440	215	-295	2	2	07-15 14:37	1	1.22	1.15	40	30
95	2000-09-17 09:00	12	33	363	133	-191	2	1	09-18 14:44	0.72	0.52	0.84	91	92
96	2001-11-05 15:00	9	36	306	149	-271	3	1	11-06 01:52	0.7	0.96	1.09	94	52
97	2001-11-24 03:00	3	15	445	141	-206	2	1	11-24 05:56	0.83	0.65	0.65	64	87
98	2003-10-28 21:00	9	36	715	322	-341	3	1	10-29 06:11	1.57	1.18	1.21	5	21
99	2003-10-30 12:00	9	39	578	308	-373	3	0	-	1.38	1.02	1.17	16	31
100	2003-11-20 06:00	9	27	578	245	-418	3	1	11-20 08:03	1.23	1.27	1.43	28	19
101	2004-07-26 21:00	15	27	363	203	-168	3	1	07-26 22:49	0.89	0.76	0.67	54	79
102	2004-11-07 09:00	18	30	363	211	-369	1	3	11-07 18:27	0.91	0.82	1.29	52	46
103	2004-11-08 18:00	24	51	363	231	-260	5	1	11-09 09:30	0.95	0.82	0.8	49	64
104	2005-05-15 00:00	6	24	365	115	-245	2	1	05-15 02:38	0.68	0.44	0.95	96	95
105	2005-08-24 03:00	6	24	363	137	-176	2	1	08-24 06:13	0.73	0.47	0.7	89	100

3. Results and Discussion

3.1. Other Geomagnetic Indices

To provide context with previous work on major geomagnetic storms, we start by investigating their effect in the more widely used geomagnetic indices for measuring and classifying storm size, namely the Kp and Dst indices. When classifying storms according to various geomagnetic indices, it is useful to recall the basic physics behind the generation of the current systems from which the associated magnetic disturbances are believed to arise.

Geomagnetic storms are well known to develop in response to enhanced solar wind energy input into the magnetosphere, which is associated with intervals of increased southward IMF and intense interplanetary electric fields (*e.g.* Gonzalez *et al.*, 1994) that drive enhanced reconnection with the magnetospheric field (Dungey, 1961). The magnetosphere responds to the increased dayside reconnection with cycles of loading and unloading of flux in the magneto-tail, *i.e.* by generating trains of substorms, and the development of intense convection and electric currents in the polar ionosphere. The increased magnetospheric convection and substorms are also associated with injection of particles from the plasma sheet into the inner magnetosphere, which intensifies the magnetospheric ring-current. The ring current reduces the Earth's magnetic field at low- and mid-latitudes, which are measured in low-latitude magnetic indices like the Dst index (Sugiura, 1964). The ring current will also affect mid-latitude magnetic disturbances, but the primary source of the mid-latitude indices during storms are the electric current systems associated with the auroral oval, in particular the substorms.

The enhanced dayside reconnection has the immediate effect of increasing the size of the polar cap, while the tail reconnection associated with the substorms causes the polar cap to contract. During geomagnetic storms, a general expansion of the polar cap and auroral oval is observed, however. The field-aligned currents in the auroral regions and the associated ionospheric currents expand toward mid-latitudes. This expansion, which is coupled with intensified currents owing to the increased substorm activity and convection, causes strongly enhanced mid-latitude geomagnetic activity as measured in geomagnetic indices such as the Kp/ap and aa indices. Several studies have shown a relation between this expansion and the Dst index (Meng, 1984; Feldstein *et al.*, 1997). The physical cause of this relation is not completely understood, but it has been suggested that the enhanced ring current during geomagnetic storms could alter the magnetic field geometry of the near-Earth magnetotail, delaying substorm onset until the open flux content of the magnetosphere grows unusually large (Nakai and Kamide, 2003; Milan, Boakes, and Hubert, 2008; Milan *et al.*, 2009).

This shows that although the variations in Dst and mid-latitude indices such as the Kp and aa index are obviously related, this relation is complex, and it is important to recall that these indices primarily measure different electric currents in the magnetosphere and ionosphere. The relation is further complicated by a relatively slow decay (*e.g.* Burton, McPherron, and Russell, 1975) of the ring current, as compared to the current systems associated with the auroral oval. This is the cause of a much stronger cumulative effect in the Dst index than in the mid-latitude indices.

The Kp index is available since 1932, and 72 of the 105 storms fall within this interval. The Dst index is available since 1957, but a revised version of Dst has recently been created, the Dcx-index. This offers an extension back to 1932 based on a slightly expanded set of stations (Karinen and Mursula, 2005). The Dcx index is highly correlated with the Dst, and in addition to offering a longer timeseries, it also provides an improved daily UT-variation (Karinen and Mursula, 2005; Mursula, Holappa, and Karinen, 2008).

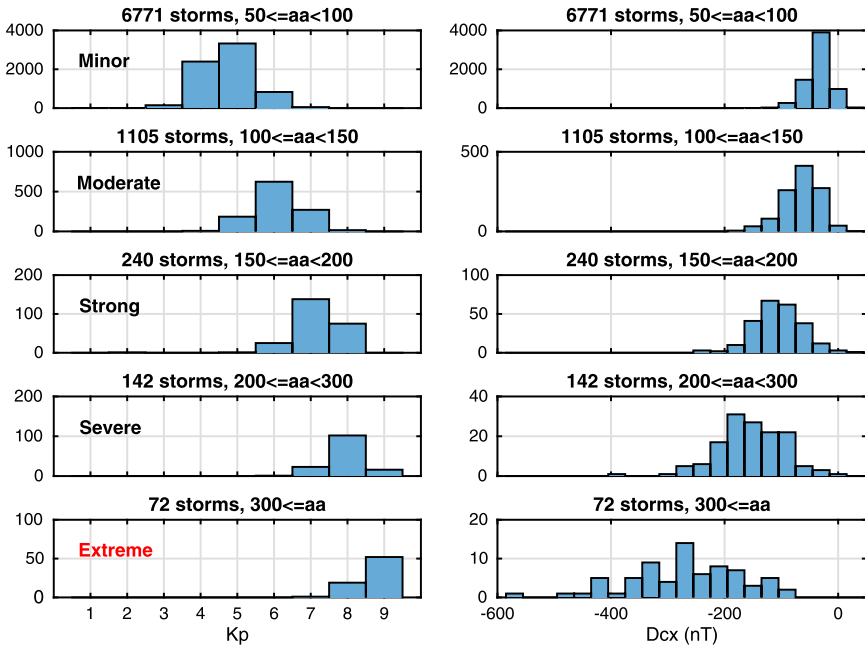


Figure 3 Histograms of peak values of the Kp index (left) and peak values of the Dcx index (right) during the storm interval, grouped according to storm peak intensity in the aa index.

Since we used an automatic procedure to identify the 105 storm intervals investigated here, the same algorithm can be used to identify intervals of storms with less intensity. We used this ability to investigate some of the characteristics of the 105 selected storms compared to the characteristics of less intense storms.

Following the frequently used procedure to group storms into three or five categories according to their intensity, we divided the identified storms into five groups according to their peak aa-value: $50 \leq aa < 100$, $100 \leq aa < 150$, $150 \leq aa < 200$, $200 \leq aa < 300$, and $300 \leq aa$, where the last storm group corresponds to our selection of 105 extreme storms. The left panel of Figure 3 shows the distribution of peak Kp values for each of these categories. The number of storms within each group in the investigated interval 1932–2010 is provided at the top of each panel. The storm groups are relatively well ordered with respect to Kp, which is expected because the aa and Kp indices are derived in a similar way. The Kp peak in the five selected aa intervals are nicely grouped around Kp values of 5, 6, 7, 8, and 9, respectively. The right-hand panel of Figure 3 shows the same, but for the low-latitude index Dcx. Again the Dcx peak intensity increases with increasing aa category, as expected. It is noteworthy, however, that an increasing spread in peak Dcx values is observed for increasing aa peaks. Particularly, our selected storm group ($aa_{\text{peak}} \geq 300$) is associated with a very large spread in Dcx peak values, from -564 nT to -86 nT. The most intense storms as measured by mid-latitude geomagnetic activity are therefore not necessarily coincident with the most intense storms as measured in low-latitude activity. The question arises whether this is only due to a limited ability of the two-station index aa to capture the global activity level. To answer this, we also investigated the range of Dcx values for all storms of Kp = 9 and found a similarly large spread in Dcx, with peaks ranging from -564 nT to -110 nT (not shown). From a physical point of view this may be expected because of the complex

relationship between the Kp/aa and Dcx index, which includes the strong cumulative effect in the Dcx index. Nevertheless, the histograms provide a new statistical quantification of these differences, even for the most intense storms. It also demonstrates that care must be taken when comparing storms classified by either the Dst or Kp/aa indices.

Another parameter based solely on the aa index that might be used as a measure of storm intensity is the peak of the 24-hour running means of aa. The use of 24-hour running means emphasizes not only the size of the peak but also the duration of the highly disturbed aa-index period. For our selected set of 105 storms the peaks of the 24-hour running means of the aa index ranges from 95 to 431. These peak values are provided in Table 2 together with the aa-index and Dcx-index peaks for each storm.

3.2. Solar Wind Sources

An important goal of the study is to identify what made the selected 105 storms so strong. To address this question, we investigated their sources in the solar wind.

3.2.1. Statistics of Direct Solar Wind Observations

Regular *in-situ* solar wind observations date back to the end of 1963. The first of our selected extreme storms for which solar wind data are available occurred in 1967. Between 1967 and 2010, 28 of the selected storms occurred, but unfortunately very many data gaps exist, particularly during the highly disturbed periods that we are interested in. Nevertheless, we statistically examined the solar wind speed and IMF intensity for the storm intervals using the OMNI hourly value dataset for 1967–2010.

Since the pioneering work of Dungey (1961), which highlighted the importance of a negative IMF Bz-component for the coupling between the solar wind and the magnetosphere, many studies have addressed the association between specific solar wind parameters and the magnetospheric response as measured in geomagnetic activity indices. Several different coupling functions of the solar wind parameters have been suggested from either a physics-based argument or from simple statistical correlation (*e.g.* Crooker, Feynman, and Gosling, 1977; Burton, McPherron, and Russell, 1975; Akasofu, 1981; Kan and Lee, 1979; Newell *et al.*, 2007 and references therein). Almost all of these involve both the solar wind speed and the southward components of the IMF, but in slightly different ways. We naturally expect our sample of extreme geomagnetic storms to be associated in general with high values of coupling parameters like vB_s , but it is interesting to see how this is reflected in the observed individual solar wind parameters for the extreme storms. Figure 4 shows histograms of the peak speed, peak IMF magnitude, and peak Bz negative during the storm intervals, again grouped according to the aa-index peak categories of the storms. Only storms without data gaps in the displayed parameter were included. This reduced the number of investigated extreme storms to 14 for the plasma observations, 16 for the magnetic field observations, and 13 where both plasma and magnetic field observations were available. Nevertheless, the trend seen in the figure is clear: For increasing storm intensity both the peak in speed and the peak in total IMF intensity tend to increase. All the extreme storm intervals had peaks in solar wind speed $v_p \geq 625 \text{ km s}^{-1}$ and IMF magnitude $B_p \geq 26 \text{ nT}$. The extreme storms apparently are not only storms where the IMF is in the optimal direction (*i.e.* predominantly southward) but also storms where the magnitude of the IMF in general is larger. It is noteworthy that the peak Bz value seems to increase significantly for the extreme storms ($aa \geq 300$) as compared to the very strong

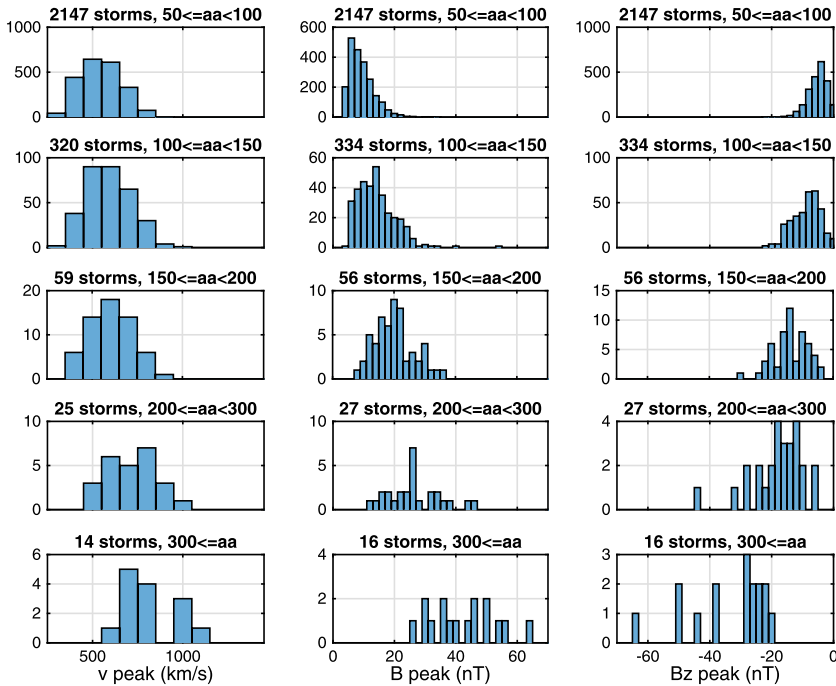


Figure 4 Histograms showing peak values of hourly solar wind parameter values during the storm interval. The parameters shown are the solar wind speed v , the IMF intensity B , and the IMF negative B_z -component. The statistics only includes storms without data gaps during the storm intervals.

storms ($200 \leq aa < 300$). Most of the very strong storms have a B_z negative peak in the interval -10 nT and -20 nT, while all the extreme storms have a B_z negative peak at or below -20 nT.

It is well documented that the stronger geomagnetic storms are generally due to solar wind disturbances created by ICMEs and their propagation through the interplanetary medium (e.g. Gosling *et al.*, 1990; Tsurutani *et al.*, 1992; Vennerstrom, 2001; Gonzalez *et al.*, 2007; Verbanac *et al.*, 2013). For the storms in the SOHO-era Richardson and Cane (2010) established a list of ICMEs based on close inspection of *in-situ* plasma and magnetic field data. Thirteen of our set of 105 extreme storms occurred in the time interval covered by this list (1996 onward), and all 13 were associated with the passage of ICMEs in this list.

It is also interesting to consider the reverse, *i.e.* how many fast ICMEs with intense magnetic fields passed Earth without generating an extreme storm. Investigating the ICME list of Richardson and Cane for 1996–2010, we searched for ICMEs satisfying the criteria of solar wind speed $v_p \geq 625$ km s $^{-1}$ and IMF magnitude $B_p \geq 26$ nT established for the extreme storms using the OMNI database. When we included both the ICME sheath region and the ejecta in the statistics, we found that 29 such ICMEs passed Earth, 16 of which were not associated with an interval of $aa \geq 300$. However, all 29 ICMEs were associated with a magnetic storm interval of moderate intensity or higher as defined above. Of the 29 ICMEs, 13 had $300 \leq aa$, 9 were in the interval $200 \leq aa < 300$, and 7 in the interval $100 \leq aa < 200$.

Table 3 Statistics of SSC occurrence in connection with storms grouped according to storm intensity, including all storms in the interval 1868–2010; storm type, aa_{peak} interval of storms of given type, total number of storms of given type N , number of storms of given type associated with SSC, N_{SSC} , given as percentage, average amplitude of SSCs (nT) Amp_{SSC} , average duration of SSCs (minutes) T_{SSC} .

Type	aa_{peak}	aa_{peak}	N	N_{SSC}/N	Amp_{SSC}	T_{SSC}
Minor	$50 \leq aa_{\text{peak}} < 100$	$50 \leq aa < 100$	10493	13 %	20	4.4
Moderate	$100 \leq aa_{\text{peak}} < 150$	$100 \leq aa < 150$	1479	34 %	25	4.2
Strong	$150 \leq aa_{\text{peak}} < 200$	$150 \leq aa < 200$	364	61 %	29	4.0
Severe	$200 \leq aa_{\text{peak}} < 300$	$200 \leq aa < 300$	227	75 %	38	3.5
Extreme	$300 \leq aa_{\text{peak}}$	$300 \leq aa$	105	91 %	56	2.7

3.2.2. Storm Sudden Commencements

Since direct solar wind observations are only available for a fraction of the period we examined, it is useful to complement them with more indirect observations. One obvious candidate for the indication of solar wind sources is the list of geomagnetic storm sudden commencements (SSCs). A typical SSC is a sudden increase in the horizontal component of the magnetic field observed at mid- and low-latitude stations, which is due to a rapid compression of the magnetosphere associated with the impact of an interplanetary shock. SSCs observed at mid- to low latitudes are therefore very good indicators of interplanetary shock arrival. Based on a pressure balance argument, the amplitude of the SSC is directly related to the dynamic pressure increase associated with the shock (Siscoe, Formisano, and Lazarus, 1968; Araki *et al.*, 1993), and it has also been shown observationally that the amplitude of the SSC is well correlated with the shock compression ratio (Cane, 1985, 1988). Furthermore, the duration of the SSC can be used to provide a rough measure of the speed of the passing shock front (Tsurutani and Lakhina, 2014).

Information on SSCs as described above is available since 1868, which makes it highly suitable for our statistical study. It should be noted, however, that only two to three ground stations detected SSCs in the early period, and for the first few years, up to 1871, only mid-latitude observatories were used.

As evaluated from the ICME list of Richardson and Cane (2010), a typical time for an ICME to pass by Earth is about one day. This means that interplanetary shocks arriving roughly between 0.5 days before the storm start and the time of the storm peak are likely to have contributed to the generation of the magnetic storm. To statistically investigate the occurrence of SSCs in relation to the occurrence of magnetic storms, we therefore determined for which storms an SSC occurred within this time interval. Table 3 lists the percentage of storms in each of the storm intensity categories for which an SSC was associated in this way. The total number of storms in each category is also given. It is clear from the table that the occurrence of SSCs in connection with the storms strongly increases with storm intensity. For the extreme storms the proportion is not far from 100 %; only nine extreme storms are not associated with an SSC on the list. The lack of an identified SSC signature, however, does not mean that these nine storms were not also associated with interplanetary shocks. Manual inspection revealed that six of these nine storms either had a very late peak or that another strong storm occurred shortly before them. Although almost all strong interplanetary shocks are associated with an SSC, an exception can occur when the magnetosphere is already disturbed (Cane and Richardson, 2003). A prominent example of this is the famous 2003 Halloween event, which was counted as two storms in this study because of the

method used to define storm intervals. In the SSC list used here, only the first Halloween storm (October 29, 2003) was found to be associated with an SSC, whereas no SSC is listed in connection with the shock passage for the second Halloween storm (October 30, 2003). However, it is well known that the second geomagnetic intensification was due to the arrival of a second CME, also associated with an interplanetary shock (Skoug *et al.*, 2004; Zurbuchen *et al.*, 2004). Two of the remaining three of the nine extreme storms that do not appear on the SSC list occurred in a recent solar cycle (April 6, 2000 and September 17, 2000), and both appear in the SOHO/CELIAS instrument interplanetary shock list and are also noted as associated with a shock in the ICME list by Richardson and Cane (2010). The last of the nine was the very first storm on the list. It occurred on May 13, 1869, at a time where ground-based magnetometer data were very rare. Taking all these specific circumstances into account, we conclude that most likely all, or almost all, of the extreme storms investigated here were associated with the passage of an interplanetary shock.

Table 3 also lists the average amplitudes and durations of the associated SSCs in each storm category. If more than one SSC was associated with a given storm, we used the SSC closest to the storm peak for the computation. Even though there is a wide spread within each category, there is also a clear tendency for increasing amplitude and decreasing duration of the SSCs with increasing storm intensity. This implies that the stronger storms tend to be associated with faster-moving shocks (short-duration SSC) with a higher compression ratio (larger-amplitude SSC) than the less intense storms. This result is readily understood from previous findings, which showed that very strong storms are closely associated with fast ICMEs that create interplanetary shocks (*e.g.* Gosling *et al.*, 1990). The passage of a fast ICME is naturally associated with high solar wind speeds and often with intense magnetic fields that occur in the passing ejecta and also in the compressed sheath region between the shock and the ejecta. When the IMF has a southward component, this will drive enhanced dayside reconnection and subsequent strong substorm activity. The results in the table statistically quantify the SSC association of the storms.

3.2.3. Storm Source Complexity

We now consider the timing between the SSC and the storm occurrence and obtain some interesting results. Figure 5 shows distributions for the storms that are associated with an SSC occurrence. The left panels show the duration of these storms as defined in this study. The vertical red lines mark the median and quartiles of the distributions. It is clear from the figure that intense storms in general last much longer than less intense storms. The median duration of the weakest storms is six hours, and this increases with storm intensity to 30 hours for the extreme storms. Moreover, the durations for the extreme storms range from 12 hours as the minimum to 93 hours as the maximum. The middle panels display the time elapsed from the occurrence of the SSC to the peak of the storm for the five different storm intensity categories (the peak taken here as the center of the three-hour interval of the aa-index peak, and the SSC is again the one closest to, and preceding, the peak). Interestingly, these distributions display only small variations from minor storms at the top to extreme storms at the bottom. We also note that the aa-index peak in the storm tends to occur quite soon after the SSC. The median lies between six to eight hours, which means that 50 % of all storms will have peaked six to eight hours after the SSC occurrence, regardless of the storm intensity. Likewise, 75–80 % of storms will have peaked within the first half day following the SSC. At first sight this may seem surprising because of the large difference in the duration of the storms, but we recall that the storm does not necessarily start at the arrival of the shock. As we defined it here, the storm starts and ends when the aa index passes the threshold of 40.

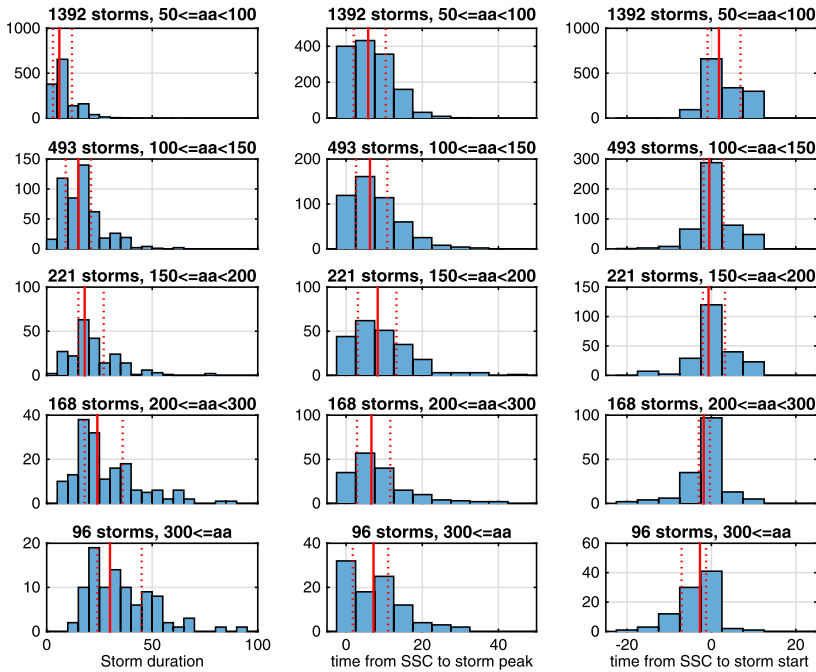


Figure 5 Left panels: Histograms of the duration of the storm periods defined as illustrated in Figure 1. Middle panels: Histograms of elapsed hours from SSC arrival to start of the storm, grouped according to storm intensity. Right panels: Histograms of time elapsed between SSC arrival and storm peak time, grouped according to storm intensity.

In contrast to the very similar distributions in the middle panels, the distributions shown in the right panels exhibit much larger differences between minor storms at the top to extreme storms at the bottom. These panels show the time elapsed between the arrival of the SSC and the start of the storm as defined here. We observe that this gradually changes from predominantly positive for the weaker storms to predominantly negative for the extreme storms. This means that for weak storms the SSC occurs before the aa index exceeds 40, while the opposite is normally the case for extreme storms. That is, the aa index exceeds 40 before or at the time when the shock closest to the storm peak arrives. Therefore, negative values indicating that the storm “starts before the SSC” occurrence simply mean that geomagnetic conditions are already active, as a result of some other solar wind disturbance, when the shock arrives. In 53 % of the extreme storms, the shock arrives in the first three-hour interval of the storm. Since the aa index is a three-hour index, it is not possible in these cases to determine whether the activity level was above storm level before the shock arrival or the shock arrival itself caused the rise in storm level activity. The shock arrived only for 5 % of these storms before the three-hour interval that marks the beginning of the storm. In the remaining 42 % the shock clearly arrived after the aa index had reached an activity level above 40. This provides an interesting clue to the key ingredients of extreme storms because it indicates that a high percentage of these storms are complex, that is, formed by two or more possibly interacting solar wind disturbances.

Many examples of interacting solar wind disturbances and the importance of a precursor southward IMF in the generation of very large geomagnetic storms are found in the literature (e.g. Tsurutani *et al.*, 1992; Gonzalez *et al.*, 2002; Wang *et al.*, 2003; Tsurutani *et al.*, 2008;

Figure 6 An example of one of the extreme storms, which is due to two interacting ICMEs. The shaded areas in the upper three panels show the interval of ejecta material according to Richardson and Cane (2010). The first ICME is compressed by the shock-sheath region of the second ICME. The vertical (red) line shows the time of the SSC occurrence created by the shock associated with the second ICME.

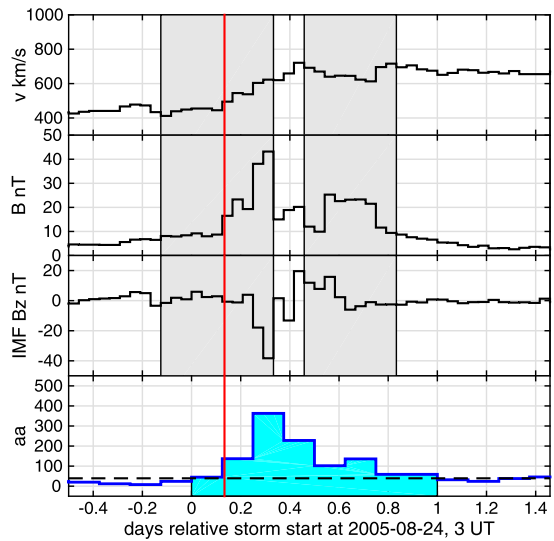


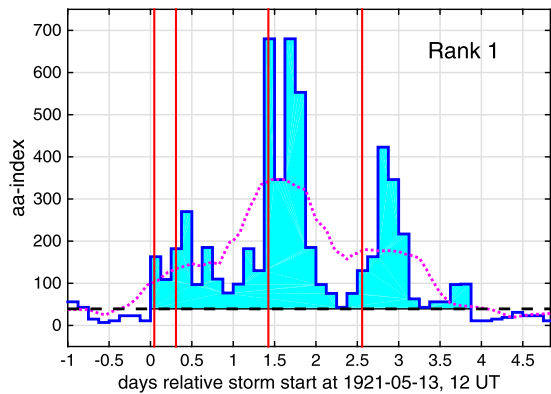
Table 4 Statistics of storm complexity inferred from geomagnetic data, including all storms in the interval 1868–2010; storm type, aa_{peak} interval of storms of given type, percentage of storms with more than one SSC (number of SSCs associated with each storm n_{SSC}), percentage of storms with only one peak within the storm interval (number of peaks associated within each storm interval n_{peak}), percentage of storms with three or more peaks within the storm interval.

Type	aa_{peak}	aa_{peak}	N	$n_{SSC} \geq 2$	$n_{peak} = 1$	$n_{peak} \geq 3$
Minor	$50 \leq aa_{peak} < 100$	$50 \leq aa < 100$	10 493	0.5 %	86 %	2 %
Moderate	$100 \leq aa_{peak} < 150$	$100 \leq aa < 150$	1 479	3 %	49 %	19 %
Strong	$150 \leq aa_{peak} < 200$	$150 \leq aa < 200$	364	7 %	39 %	33 %
Severe	$200 \leq aa_{peak} < 300$	$200 \leq aa < 300$	227	12 %	36 %	39 %
Extreme	$300 \leq aa_{peak}$	$300 \leq aa$	105	25 %	14 %	57 %

Zhang, Richardson, and Webb, 2008; Gonzalez *et al.* 2011a, 2011b). Figure 6 shows an example of the extreme storms investigated here, the storm that occurred on August 24, 2005. The two shaded areas are ejecta regions identified by Richardson and Cane (2010). The figure shows that the storm is caused by two interacting ICMEs. The shock (SSC marked by the red vertical line) from the second ICME acts to compress the ejecta of the first ICME (gray area on the left), thereby increasing the IMF intensity and hence the IMF Bz component. In addition to the effect of the compression, interplanetary shocks can also deflect the magnetic field direction, and the interplanetary field lines are draped around the ejecta. These effects can both decrease and increase the southward component of the IMF (*e.g.* Wu and Dryer, 1996).

Even when no solar wind data are available to interpret the cause of the storm, it is still possible to glean some information about the complexity of the sources simply by counting the number of SSCs associated with the storm, and also the number of individual local peaks in *aa* during the storm interval. Table 4 shows that the fraction of storms with more than one associated SSC increases with storm level from 0.5 % for the minor storms to 25 % for the extreme storms. When we use the number of individual geomagnetic peaks as a measure of

Figure 7 The aa-index variations and SSCs associated with the highly complex storm at the top of the ranking list. The storm started on May 13, 1921.



the complexity, we again find a rapidly increasing fraction of complexity with storm level. Table 4 shows that only 14 % of the extreme storms have only a single peak in the aa index, but 86 % of the minor storms are of this type. Observing two individual peaks in the storm interval is not necessarily an indication of a complex source, however, because single ICMEs are often associated with two individual geomagnetic peaks, one due to the sheath region and one due to the ejecta itself (e.g. Kamide *et al.*, 1998). Likewise, the presence of only one or two peaks does not necessarily exclude the presence of multiple sources in the solar wind if they arrive in close succession. However, events with more than two individual peaks are highly likely to be associated with multiple sources in the solar wind, interacting or not. The statistics presented here shows that 57 % of the extreme storms are of this type.

An illustrative early example of a highly complex storm caused by multiple solar wind disturbances is the storm at the top of the list in the geomagnetic ranking. This is the so-called New York Railroad Storm that commenced on May 13, 1921. This storm lasted almost four days and caused serious disruptions in the New York railroad signal and switching system. It is depicted in Figure 7. No fewer than four SSCs were observed within the storm interval, along with eight individual peaks in the aa index. Had each of these peaks occurred alone, three would have been classified as strong storms, one as a severe storm, and three as extreme storms. Second on the geomagnetic ranking list is the famous Quebec storm that occurred on March 13, 1989, which caused a power blackout in the entire Quebec region. This storm was associated with two SSCs and five individual peaks.

3.2.4. Forbush Decreases

Another way to obtain indirect information about the solar wind associated with the storms is to examine ground-based neutron monitor data for the occurrence of Forbush decreases (FDs). Short-term decreases of galactic cosmic rays (GCRs), with durations of the order of days, were first observed by Forbush (1937), and are generally believed to be caused by strong disturbances in the interplanetary magnetic field associated with interplanetary shocks and ICMEs and also co-rotating interaction regions (CIRs) (e.g. Cane, 2000 and references therein, Dumbović *et al.*, 2012). They have been monitored continuously by ground-based neutron monitors since the 1950s, *i.e.* before the first *in-situ* measurements of the solar wind, which makes them highly useful for this study. As mentioned in Section 2.1, we used neutron monitor (NM) data from nine individual observatories to investigate the possible occurrence of FDs during intense geomagnetic storms. This provides data coverage for all our extreme storms from September 1957 onward, covering 46 storms.

To reduce the effects of daily variations, we calculated an average over three NM stations of roughly similar cutoff rigidity, but different longitudes of asymptotic arrival directions (see *Dumbović et al., 2011*). The cutoff rigidity of the station is an important factor that determines the magnitude of the observed FD. It is the smallest momentum per charge that a particle must have to reach a certain geographical location (*e.g. Cooke et al., 1991; Smart, Shea, and Flückiger, 2000*). Since particles can enter the atmosphere more easily at the poles and high latitudes than at the equator and low latitudes, FDs are rigidity dependent (*e.g. Cane, 2000*). Because the availability of data in the early years is limited (1950s and 1960s in particular), the difference in the rigidities between stations used can be as much as 3.4 GV, which can have a substantial influence on the measured FD magnitude (see *e.g. Cane, 2000*). However, for the majority of events (72 %) the difference in rigidities between stations is lower on average than the daily variations.

Neutron monitor data were available for all 46 extreme storms that occurred after September 1957, and we found FDs overlapping the storm interval for all of these 46 storms. For 41 events (89 %) we found that the FD onset occurred after the start of the storm, as recorded in the aa index, but before or within the three-hour interval of maximum aa (seven events in the three-hour peak interval). This is in close accordance with the results on the SSC timing described above and reinforces the interpretation that for most of the extreme storms the geomagnetic activity is already elevated when the ICME associated with the storm maximum arrives. The FD onset occurred in only three cases before the magnetic storm start, and in two cases the FD onset occurred after the maximum of the storm. The average time difference between the storm start and the FD onset was five hours, and the average time difference between the FD onset and the aa maximum was nine hours (the aa-index timing here taken as centered on the aa-max three-hour interval).

The onset times, magnitudes, and duration of the FDs for the individual storms are provided in Table 5. The magnitude was measured as the absolute value of the relative decrease from the onset value to the deepest minimum. The average magnitude is 7.6 %, which is about twice the value for average ICME-associated FDs obtained, for example, in *Dumbović et al. (2011)* or *Richardson and Cane (2011a, 2011b)*, and is close to the FD size of 8.3 % obtained by *Cane, Richardson, and Rosenvinge (1996)* for cases when both shock and ejecta are intercepted. It should be noted that an extreme magnetic storm will significantly change (most likely reduce) geomagnetic shielding and hence the cutoff rigidity applicable to neutron monitors. Since the reduced cutoff rigidity leads to enhanced GCR flux masking the depression of the GCR intensity, this effect somewhat weakens the observed Forbush decrease magnitude (*e.g. Chilingarian and Bostanjyan, 2010; Dumbović et al., 2012*). Despite this, we found that FDs associated with the largest geomagnetic storms are substantially larger than average ICME-associated FDs. Therefore, our analysis provides strong evidence that the largest geomagnetic storms are associated with deeper galactic cosmic-ray depressions and that their interplanetary sources are most likely fast shock-associated ICMEs with strong magnetic fields.

3.2.5. Energetic Particle Events

Observations of energetic particles generated as a consequence of solar eruptions also provide knowledge about the source of the geomagnetic storms. We have investigated whether the geomagnetic storms under study were accompanied by energetic storm particle (ESP) events, that is, by an increase in the intensity of energetic particles associated with the passage of an interplanetary shock (*e.g. Cohen, 2006*). It is generally considered that the ESP events are charged particles trapped in the vicinity of an interplanetary shock by self-generated waves and are transported with it (*e.g. Bryant et al., 1962*). This provides a good

Table 5 Cosmic-ray and energetic particle characteristics of the extreme storms; chronological storm number n , storm start time in format YYYY-MM-DD HH:MM, time difference between storm start and storm peak in hours h_{peak} , time difference between storm start and FD onset in hours h_{FD} , total magnitude of FD in percent Mag_{FD} , duration of FD in days T_{FD} , indicator (Yes/No) of GLE occurrence in association with storm GLE , indicator of ESP occurrence for storms associated with SSC ESP , Dcx-index peak (nT), rank based on aa index and all observatories similar to Table 2, *total rank*.

n	Storm start time yyyy-mm-dd hh:mm	h_{peak}	h_{FD}	Mag_{FD}	T_{FD}	GLE (Y/N)	ESP (Y/N)	Dcx peak	Total rank
59	1957-09-04 12:00	3	0	10.1	12.21	N	–	–320	36
60	1957-09-13 00:00	9	–1	2.5	4.38	N	–	–419	41
61	1957-09-29 03:00	12	9	7.2	3.83	N	–	–250	58
62	1958-02-10 15:00	9	8	6.2	4.88	N	–	–421	23
63	1958-07-08 06:00	9	1	6.2	3.54	N	–	–321	15
64	1958-09-04 12:00	3	9	3.6	4.17	N	–	–301	53
65	1959-03-26 06:00	33	1	8.1	6.17	N	–	–242	70
66	1959-05-11 21:00	18	–2	12.7	7.21	N	–	–87	104
67	1959-07-15 06:00	9	1	18.7	2.33	Y	–	–418	9
68	1959-07-17 15:00	3	0	22.4	6.88	N	–	–167	74
69	1960-03-31 03:00	36	6	11.9	8.67	N	–	–327	16
70	1960-04-29 00:00	39	35	6.7	4.08	N	–	–316	29
71	1960-10-05 21:00	24	8	6.6	4.29	N	–	–271	45
72	1960-11-12 12:00	18	4	–	2.88	Y	–	–310	28
73	1960-11-15 12:00	12	1	–	5.38	Y	–	–174	90
74	1961-07-27 03:00	6	–8	7.3	6.46	N	–	–143	97
75	1961-10-28 06:00	12	6	2.3	3.08	N	–	–274	65
76	1963-09-21 12:00	33	32	8.6	8.92	N	–	–224	75
77	1967-02-16 06:00	3	–7	4.7	5.42	N	–	–122	105
78	1967-05-25 09:00	12	5	7.2	11.29	N	–	–375	13
79	1969-02-02 15:00	3	4	1.2	3.33	N	–	–181	101
80	1970-03-07 12:00	30	27	4.0	9.96	N	–	–283	55
81	1972-08-04 12:00	9	8	20.8	10.42	Y	–	–110	56
82	1981-07-25 03:00	9	7	8.8	6.75	N	Y	–209	51
83	1982-07-13 03:00	18	11	21.1	12.83	N	Y	–326	27
84	1982-09-05 21:00	15	1	8.3	7.17	N	Y	–265	39
85	1986-02-07 09:00	33	32	9.6	7.25	N	no SSC	–268	26
86	1989-03-13 00:00	21	6	14.0	12.13	N	Y	–565	2
87	1989-10-20 06:00	12	7	13.4	10.17	Y	N	–274	63
88	1989-11-17 06:00	12	0	2.6	2.25	Y	N	–254	78
89	1991-03-24 03:00	0	11	15.7	5.88	N	Y	–284	59
90	1991-06-04 12:00	27	0	21.0	17.13	N	N	–202	57
91	1991-11-08 06:00	15	3	7.2	3.50	N	N	–366	34
92	1992-09-09 00:00	9	2	5.9	6.33	N	N	–123	99
93	2000-04-06 15:00	6	0	2.4	3.54	N	no SSC	–294	83
94	2000-07-15 03:00	12	7	13.4	4.13	Y	Y	–295	30
95	2000-09-17 09:00	12	5	6.4	7.00	N	no SSC ^a	–191	92
96	2001-11-05 15:00	9	8	9.4	6.50	Y	Y	–271	52

Table 5 (Continued.)

<i>n</i>	Storm start time yyyy-mm-dd hh:mm	h_{peak}	h_{FD}	Mag_{FD}	T_{FD}	GLE (Y/N)	ESP (Y/N)	Dcx peak	Total rank
97	2001-11-24 03:00	3	1	6.9	4.33	N	Y	-206	87
98	2003-10-28 21:00	9	8	22.1	22.12	Y	Y	-341	21
99	2003-10-30 12:00	9	3	22.1	22.12	Y	no SSC	-373	31
100	2003-11-20 06:00	9	1	4.8	9.04	N	N	-418	19
101	2004-07-26 21:00	15	2	12.7	3.92	N	Y	-168	79
102	2004-11-07 09:00	18	5	6.0	2.17	N	Y	-369	46
103	2004-11-08 18:00	24	24	10.1	8.63	N	Y	-260	64
104	2005-05-15 00:00	6	1	11.0	11.17	N	Y	-245	95
105	2005-08-24 03:00	6	2	5.6	5.25	N	Y	-176	100

^aSSC occur after peak.

physical explanation of the ESP association with shocks and why they are more frequently observed up to energies of a few MeV. These low-energy particles have a lower probability of escaping the turbulent region near the shock (*e.g.* Reames, 1999). This turbulent trapping of particles is also of vital importance for the shock acceleration process itself (Lee, 2005). Starting from the sublist of identified geomagnetic storms described above in which an SSC was recorded, we used the SEPTEM dataset described in Section 2.1 for our analysis. Energetic particle observations as measured by near-Earth spacecraft (GOES and IMP8) during the time interval of the storm and the associated SSCs were examined for each storm. The list of the selected geomagnetic storms spanned from February 1973 until September 2005. No SEPTEM data were available before November 1973.

For each of these geomagnetic storms, we plot the SEPTEM proton intensity *versus* time and examine whether an ESP enhancement associated with the corresponding SSC was observed near Earth. Figure 8 shows an example of an identified ESP event on October 29, 2003, based on five-minute-averaged intensities of 5–200 MeV protons in ten energy channels from 00:00 UT on October 28, 2003 to 00:00 UT on October 30, 2003. The dashed vertical line denotes the time of the SSC occurrence associated with the extreme magnetic storm taking place during this period (the Halloween storm). An intense SEP event was observed in response to the X17.2 solar flare and the fast halo-CME that occurred on October 28, 2003 (Malandraki *et al.*, 2005). The observations in Figure 8 show that although the high-energy intensity profiles start gradually to decay, the lower energy channels (> 5 MeV) exhibit an additional ESP intensity enhancement, peaking at the time of the SSC (06:11 UT) and associated shock passage at Earth. The ESP increases are more prominently observed up to energies of ~ 46 MeV.

In Figure 9 an SEP event began at 06:00 UT on May 22, 2002 and was associated with a fast halo-CME and a C5 flare (Cane, Richardson, and Rosenvinge, 2010). An ESP enhancement associated with the SSC at 10:50 UT on May 23, 2002 is also evident. The intensity increase related to the local shock passage was observed at unusually high energies (~ 95 MeV). Furthermore, although this ESP event morphologically appears to have a spiky structure (Sarris and van Allen, 1974), its duration is very long (several hours). Huttunen-Heikinmaa and Valtonen (2009) have reported a clearly identified ESP event for this period that is associated with a fast forward-IP shock observed at 10:15 UT on May 23, 2002 at the L1 Lagrangian point. The SSC observed at Earth 35 minutes later is apparently caused by

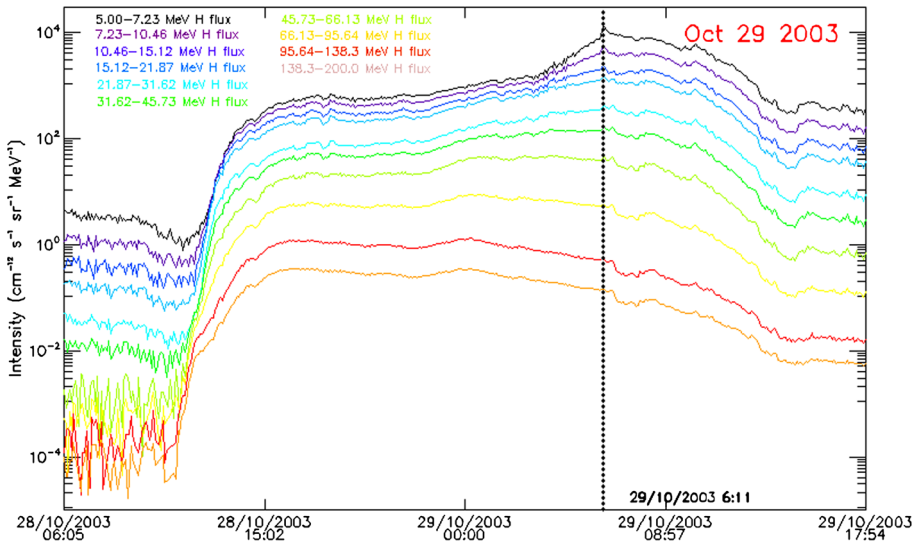


Figure 8 Identified ESP event on October 29, 2003 based on SEP-EM five-minute-averaged intensities of 5–200 MeV protons (see text). The dashed vertical line denotes the time of the SSC occurrence associated with the extreme magnetic storm taking place during this period.

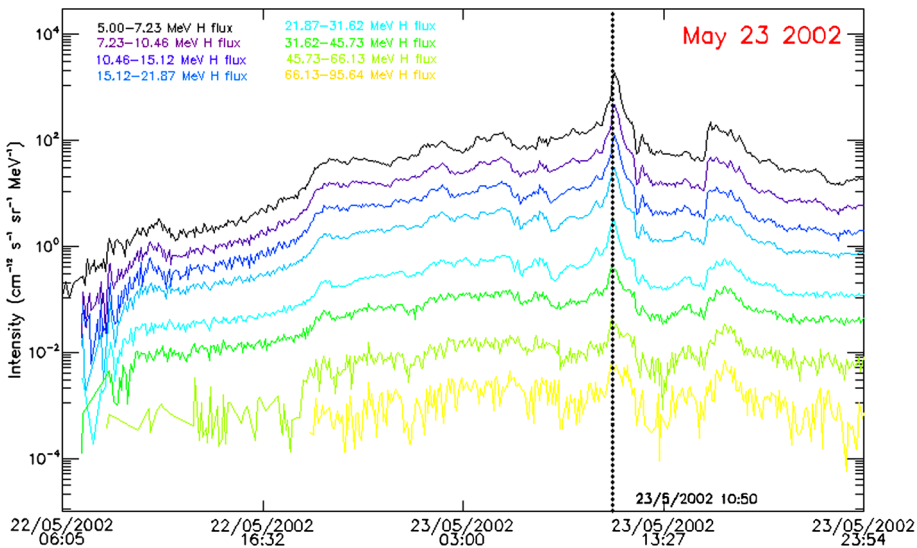


Figure 9 Identification of an ESP enhancement event associated with an SSC at 10:50 UT on May 23, 2002 shown in the same format as Figure 8.

the fast forward-shock able to abundantly accelerate energetic protons. This event does not appear on our list of extreme storms.

In compiling the list of associated ESP events in this work, we also verified our results by extensively cross-checking and enhancing the list with ESP events that have been identified in the literature for both the recent Solar Cycle 23 and earlier periods in the space era (*e.g.*

Table 6 Statistics of ESP occurrence for all storms in the interval 1973–2005; storm type, aa_{peak} interval of storms of given type, number of storms associated with SSC N_{SSC} , number of SSC associated storms with ESP occurrence N_{ESP} , N_{ESP} given as percentage $N_{\text{ESP}}/N_{\text{SSC}}$.

Type	aa_{peak}	N_{SSC}	N_{ESP}	$N_{\text{ESP}}/N_{\text{SSC}}$
Minor	$50 \leq aa_{\text{peak}} < 100$	368	111	30 %
Moderate	$100 \leq aa_{\text{peak}} < 150$	216	71	33 %
Strong	$150 \leq aa_{\text{peak}} < 200$	68	35	52 %
Severe	$200 \leq aa_{\text{peak}} < 300$	49	31	63 %
Extreme	$300 \leq aa_{\text{peak}}$	20	14	70 %

Klecker *et al.*, 1981; van Nes, Roelof, and Reinhard, 1984a; van Nes *et al.*, 1984b; Beeck and Sanderson, 1989; Kallenrode, 1995; Huttunen-Heikinmkaa and Valtonen, 2009; Mäkelä *et al.*, 2011). Table 5 includes information on ESP occurrence for the extreme storms that occurred after 1973.

Table 6 shows the results of the statistical analysis of storms of all intensities that occurred after 1973. Seventy percent of the investigated extreme storms, *i.e.* the extreme storms with available SEP-EM-data that were associated with an SSC, were found to be associated with an ESP-event. The table also shows that the percentage of ESP association increases with storm intensity. Thirty percent of the minor storms are found to be associated with an ESP-event, but we recall that only SSC-associated storms were included in the statistics, and for the minor storms this is only a small percentage (13 % according to Table 3). The association between ESP-occurrence and storm intensity can be understood within the general consensus that strong storms are associated with the passage of fast ICMEs that are assumed to drive strong interplanetary shocks. This is in good accordance with the results presented in Section 3.2, emphasizing the role of shocks in enhancing pre-existing magnetic field disturbances in the solar wind. The high solar wind speed behind the shock coupled with a possibly enhanced southward IMF will drive strong dayside reconnection, which then leads to strong substorm activity.

3.2.6. Long-Term Variations

The set of extreme storms was derived from a time-series of almost 150 years. This gives us the opportunity to investigate long-term variations of the storm occurrence. Figure 10 shows the distribution of storm occurrences relative to the solar cycle and the evolution of solar activity over the century. A scaled version of the sunspot number is shown for direct comparison. The extreme storms are shown as bars in the top panel. It is clear from the figure that extreme storms occurred in all cycles in the period, even in the very weak cycles at the beginning of the century. The very weak Solar Cycle 14 that started close to the turn of the twentieth century featured no fewer than two storms that appear in the top 10 list in the ranking, namely the storms in October 1903 and September 1909, which are ranked as numbers 6 and 3 in the total ranking-list. For comparison, the highest ranked modern storm in the SOHO-era, the well-known Halloween storm, is ranked as number 19. Nevertheless, the three cycles occurring from the 1940s to the 1960s, *i.e.* Cycles 17–19, and also the recent Solar Cycle 23, appear to have been richest in extreme storms. Strong activity cycles in general appear to foster more extreme storms than the weaker cycles, but the pattern is not very clear, probably because extreme storms are relatively rare.

The extreme storms also occurred in all phases of the solar cycle, *i.e.* not just during solar maximum and in the declining phase where geomagnetic activity is usually strongest,

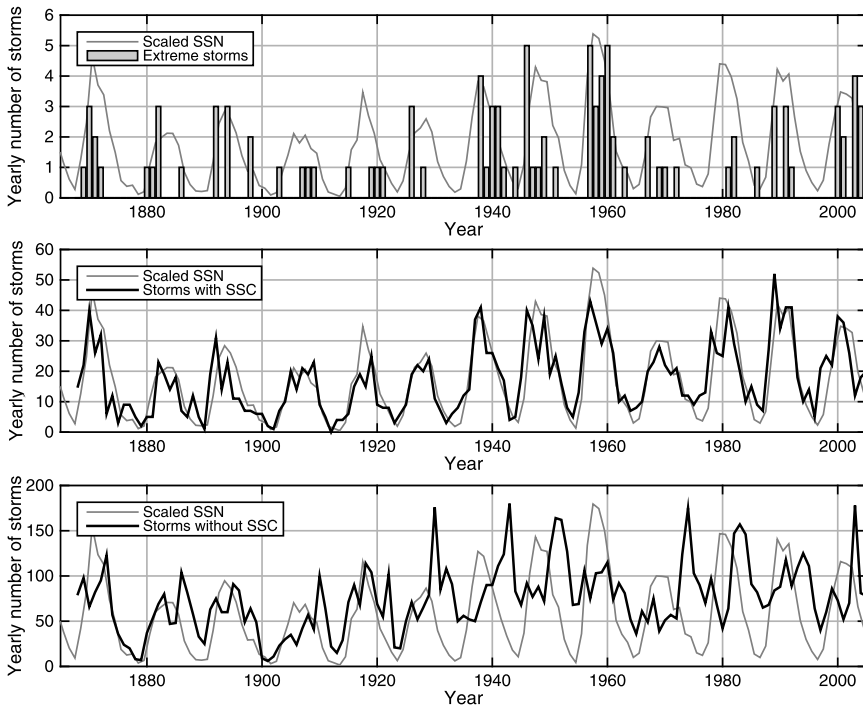


Figure 10 Long-term variations of the number of storms compared with the (scaled) sunspot number. (Top) The yearly number of extreme storms, displayed as bars. (Middle) The yearly number of storms associated with SSCs. (Bottom) The yearly number of storms without any associated SSC.

but also frequently in the rising phase and even, at more than one occasion, close to solar minimum.

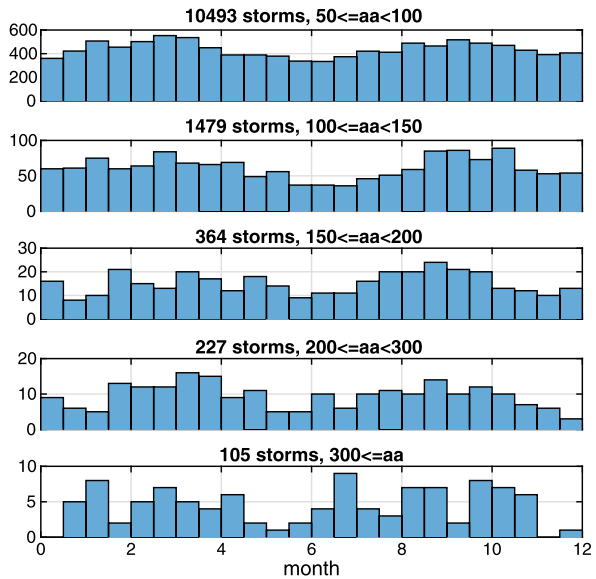
For comparison, the second and third panel show the yearly number of all the storms observed regardless of storm intensity. The middle panel shows the storms that were also associated with an SSC as defined above, while the bottom panel shows the storms that were not associated with an SSC. It is clear that the solar cycle variation of the two types of storms is very different. The SSC-associated storms closely follow solar activity as measured by the sunspot number, both the solar cycle variation and the longer-term variation in the size of the maximum. Notably the yearly number of these storms is also relatively close to zero during solar minimum. This is very different from geomagnetic activity in general. Mid-latitude indices such as the aa index are well known to display strong peaks in the declining and late declining phase of the cycle (e.g. Feynman and Crooker, 1978; Legrand and Simon, 1981). The number of storms not associated with SSCs shown in the bottom panel display a pattern that is primarily characterized by strong peaks in the declining and late phase of the cycle. This resembles the well-known long-term variation in the aa index. The curves in the middle and bottom panel for the interpretation well that the SSC-associated storms are mainly due to ICMEs, while the storms not driving SSCs are mainly associated with corotating interaction regions (CIRs) and high-speed streams from coronal holes: CIRs and high-speed streams from coronal holes are known to generate strong geomagnetic activity, mainly in the declining and late declining phase of the cycle, while ICME occurrences are most frequent close to solar maximum and in the early declining phase.

The aa index also displays a significant long-term increase during the twentieth century, including an increase of the activity during solar minima. This increase has been attributed to both a general rise in the solar wind speed and a general rise in the heliospheric magnetic field (Feynman and Crooker, 1978; Lockwood, Rouillard, and Finch, 2009; Svalgaard and Cliver, 2010, and references therein). The rise during solar minima is also clearly visible in the yearly number of storms not associated with SSCs. This type of effect, that the number of storms is associated with the background solar wind level, has also been observed in previous studies, where the number of storms is defined as the number of times the activity exceeds a given threshold. In this case the number of storms has been found to be highly correlated with the general activity level (Cliver *et al.*, 1999; Vennerstroem, 2000). CIRs are created as a compression of the background solar wind caused by the high-speed streams, which means that a general increase in the heliospheric magnetic field (and speed) will create more and stronger CIR-related storms. Still, we recall that the association between storms with or without SSCs with ICME- and CIR-driven storms, respectively, is of course not perfect. Not all geo-effective ICMEs drive shocks with associated SSCs, and conversely, CIRs can be associated with SSCs (Richardson *et al.*, 2006), although this is rare.

We now turn to another well-known type of long-term variation relevant for our dataset, namely the so-called semiannual variation of geomagnetic activity, *i.e.* the tendency for geomagnetic activity to be weaker close to the solstices than close to equinoxes. It has been known for long that geomagnetic storm occurrence also follows this pattern (Newton, 1948; Gonzalez *et al.*, 1993), but no general consensus has been reached concerning the source (Svalgaard, Cliver, and Ling, 2002). Semiannual activity in general is usually attributed to one or more of three independent effects: the Russell–McPherron effect, which points to a half-year variation in the southward IMF component that is due to the general geometry of the solar wind in GSM-coordinates (Russell and McPherron, 1973), the equinoctial hypothesis, pointing to a less effective coupling of solar wind and the magnetosphere and possibly also a coupling of magnetosphere and ionosphere during solstices (Bartels, 1932; McIntosh, 1959; Svalgaard, 1977), and the axial hypothesis (Cortie, 1912; Bohlin, 1977), which points to the Earth's movement in and out of the solar equatorial plane, leading to a semiannual variation in solar wind speed (*e.g.* review by Gonzalez *et al.*, 1993; Cliver, Kamide, and Ling, 2002, and references therein). In recent years, it was realized that geomagnetic storms play a prominent role in establishing this pattern (Crooker, Cliver, and Tsurutani, 1992; Svalgaard, Cliver, and Ling, 2002) and that the effect increases with storm intensity (Svalgaard, Cliver, and Ling, 2002). Crooker, Cliver, and Tsurutani (1992) attributed the effect on large storms (measured by Dst) mainly to the Russell–McPherron effect that acts in the sheath region preceding the ejecta, while Svalgaard, Cliver, and Ling (2002) demonstrated that the larger part of the storm effect can be explained by variations in the angle between the solar wind direction and the Earth dipole axis, indicating a significant influence of this angle on the coupling efficiency of the solar wind and the magnetosphere.

Figure 11 shows the yearly distributions of the number of storms for the storm set investigated here. We divided the storms into our five categories of storm intensity, and the results confirm the finding by Svalgaard, Cliver, and Ling (2002). We find a semiannual effect at all storm levels that seems to increase with storm intensity, although a larger number of extreme storms would have been desirable to consolidate the statistics. In Figure 12 we show the same data, but now separated into storms with and without associated SSC, *i.e.* separated into what we interpret as ICME-dominated and CIR-dominated storms. In this figure we chose to consolidate the statistics by rebinning the data in larger bins for the strong to extreme storms. For the strong storms there are now two bins per season, and for the severe and extreme storms there is a single bin per season. Following Cliver,

Figure 11 Yearly distributions of the number of storms, provided in half-monthly intervals and shown for different storm intensities. The distributions show a clear semiannual component.



Kamide, and Ling (2002), we chose to center the seasons at the equinoxes and solstices, but slightly different choices do not significantly alter the statistics. We note that the winter bin appears as two bins in the beginning and end of the year, but it is indeed a single bin displayed as two. Interestingly, the semiannual variation seem to disappear completely for the weaker SSC associated storms (left upper panels). A clear semiannual variation is observed only for SSC storms with peaks larger than 150. This is the opposite for the non-SSC-associated storms displayed in the right columns. Here a clear semiannual wave is observed for both the weaker and stronger storms. We recall that the nine extreme storms in the bottom panel are most likely all shock associated and therefore very likely ICME associated. It seems difficult to explain these results from one of the proposed mechanisms alone. The absence of a semiannual wave in the weak SSC-associated storms combined with its presence in the similar storms without SSC seems to point toward the compression of the background (Parker spiral) solar wind in the CIRs or the high speeds in the following high-speed streams as the source of the semiannual variation. This again would point toward either the Russell–McPherron mechanism or the axial hypothesis as the most probable explanation. On the other hand, this cannot readily explain the clear semiannual effect in the strong to extreme storms with SSC, except through a Russell–McPherron effect in the sheath region as suggested by Crooker, Cliver, and Tsurutani (1992). We recall, however, that their study was based on the more cumulative Dst index, where the sheath region rise in the Dst index was able to contribute to the later peak within the ejecta region. For the aa index the magnetospheric decay-time is much shorter, therefore the peak solar wind input in our case should occur in the sheath for this mechanism to work. We have shown above that this can occur for ICME–ICME interactions where the leading ICME ejecta is compressed in the sheath of the trailing ICME (see Figure 6), but this is different from, and likely more effective than, a Russell–McPherron effect arising from increased B_s that is due to compression and deflection of the background IMF. In contrast, the equinoctial hypothesis seems to be able to explain most of the effect for the intense storms, as well as the effect in the weak storms that are not associated with SSCs (Svalgaard, Cliver, and Ling, 2002; Cliver, Kamide, and Ling, 2002). However, it does not explain why the minor to moderate

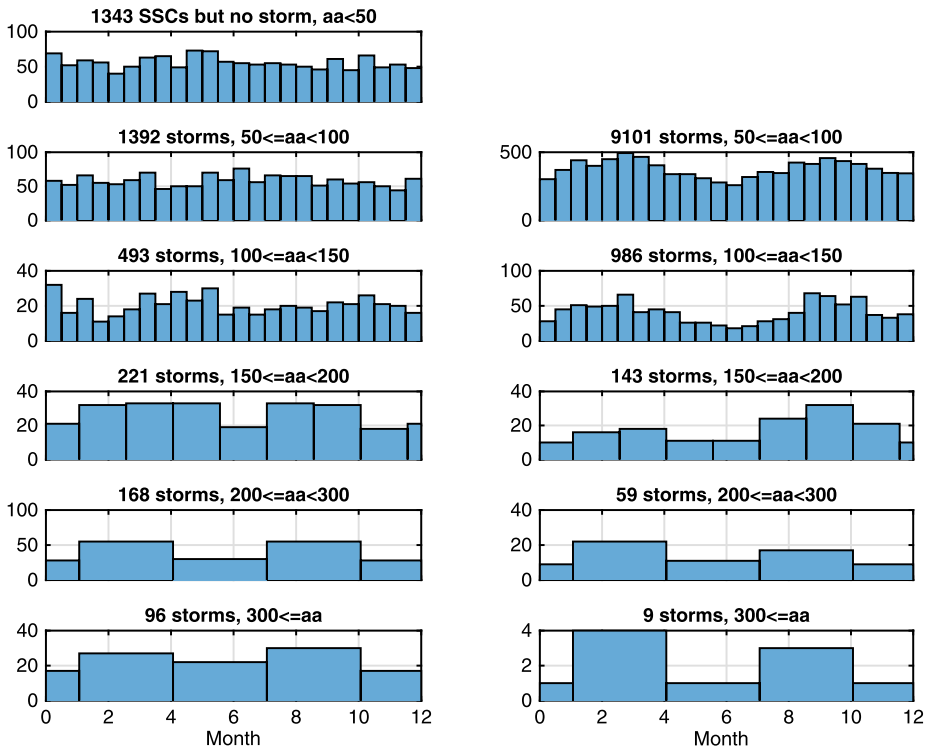


Figure 12 Yearly distributions of the number of storms similar to Figure 11, but here the storms were divided into SSC-associated storms (left panels) and storms not associated with any SSC (right panels). For reference, we show in the top panel to the left the yearly distribution of SSCs that were not geo-effective, *i.e.* were not associated with a geomagnetic storm.

SSC associated storms do not show any semiannual variation. Why should the solar wind coupling during solstices be more efficient for these mainly ICME-driven storms than for the storms driven by CIRs and high-speed streams? More detailed studies of the coupling of the solar wind magnetosphere and ionosphere during solstice versus equinox conditions are clearly needed for a full understanding of this phenomenon.

4. Summary and Conclusions

In summary, we have investigated all extreme geomagnetic storms that occurred between 1868–2010, here defined as storms with a peak in the aa index larger than or equal to 300. In total, this constitutes 105 storms. We investigated and ranked the storms by including a wide variety of supplementary data. We thereby set recent well-investigated extreme storms, which have caused space weather hazards for modern technology, in relation to the occurrence of similar or larger storms in the past. We were also able to quantify many known tendencies. We find the following.

- The New York Railroad Storm that occurred on May 13, 1921 is the highest ranked storm when the storms are ranked according to the aa index supplemented by nine series of single observatory data. The Quebec storm on March 13, 1989 is ranked second.

- The weak solar cycle in the beginning of the twentieth century fostered two storms that are ranked higher than any of the well-known extreme storms of the recent Cycle 23.
- Extreme storms defined by their peak intensity in mid-latitude geomagnetic indices (aa/Kp) display a wide variety of ring-current (Dcx/Dst) intensities with peaks ranging from -564 nT to -86 nT.
- The observed minimum IMF peaks for all extreme storms for which *in-situ* solar wind data were available without gaps throughout the storm interval were $B \geq 26$ nT and $B_z \leq -20$ nT (hourly averages). Similarly, the observed minimum of the peak solar wind speed was $v \geq 625$ (hourly averages).
- All the extreme storms that were covered by the Richardson and Cane ICME list were found to be associated with ICMEs. Conversely, 29 events were found on the ICME list with a solar wind speed and magnetic field intensity exceeding the minimum found in the extreme storm list. Somewhat fewer than half, namely 13, were associated with extreme storm values, but all 29 were associated with aa-index values above 100.
- The large majority (> 91 %) of the extreme storms are associated with interplanetary shocks, as indicated by SSC occurrence.
- Of the extreme storms found to be associated with SSCs, 70 % were found to be also associated with an ESP event.
- All storms for which FD-data were analyzed (all extreme storms occurring after 1957) overlapped in time with a Forbush decrease, and the average magnitude of these FDs was about twice the average value of FDs overall.

To place the extreme storms in context with less intense storms, we also identified all storms ($aa_{\text{peak}} \geq 50$) that occurred since 1868 and paired them with SSC occurrence. For the later periods solar wind and ESP occurrence was also investigated for all storms. These results have important implications for space weather forecasting. When we compare extreme storms statistically by grouping the storms according to storm intensity, we find the following.

- In this study storms were defined to start and end when the aa index passed the threshold of 40. In this way, the duration of the storms increases significantly with storm intensity, from a median value of 6 hours for the minor storms to 30 hours for the extreme storms.
- The characteristics of extreme storms, *i.e.* SSC association, ESP association, large peak IMF and high solar wind speed, and complexity of the geomagnetic signal all decrease with decreasing storm intensity, as expected. We quantified these tendencies.
- For the extreme storms the threshold of 40 is most often exceeded either before or in the three-hour interval where the (last) SSC occurs, *i.e.* the storm starts immediately upon arrival of the SSC or earlier. In only 5 % of the events is the aa index lower than 40 in the three-hour interval in which the SSC arrive. In contrast, for the minor to strong storms, this percentage is roughly 40–60 % and the percentage decreases with increasing storm level.
- We find that the yearly occurrence of all SSC-associated storms, interpreted as indicative of the number of geo-effective ICMEs associated with shocks, roughly follows the sunspot cycle, including the variation of maxima from cycle to cycle.
- We confirm previous findings that the storm occurrence displays a semiannual variation that increases with storm intensity. However, a notably new result is that this variation appears to depend on the storm source. For SSC-associated storms of minor to moderate intensity, the majority of which are believed to be caused by ICMEs, the storm occurrence is relatively uniformly distributed over the year, displaying no semiannual variations. This is in contrast to the storms without SSCs, which are believed to be mainly due to high-speed streams and CIRs. For these storms a clear semiannual variation is observed for the

weaker storm classes. For the stronger storms, however, a clear semiannual signature is observed both for storms with and without SSC-association. These results cannot readily be explained by existing theories for semiannual variation of geomagnetic activity.

The complexity and timing analysis, in particular, also provided interesting new characteristics with respect to the causes of the extreme storms, indicating that many storms were associated with multiple, possibly interacting, solar wind disturbances.

- The extreme storms are mostly complex with several individual peaks and frequently more than one associated shock. Specifically, 57 % are associated with three peaks or more, and 25 % with two or more SSCs.
- For a large part of the extreme storms geomagnetic conditions are already active (the aa index is higher than twice its average value at 40) when the main disturbance arrives. This is confirmed in the timing analysis for both SSCs and Forbush decreases. For 42 % of the SSC-associated storms, the SSC arrives after the three-hour aa-index interval that marks the start of the storm. For the FD onsets the corresponding ratio is 59 %.
- For another similarly large fraction of the extreme storms, the storm starts immediately in association with the disturbance arrival. That is, the SSC or FD onset occurs within the first three-hour interval of the storm. For the SSCs this is the case for 53 % of the storms, and for the FD onsets it occurs in 30 % of the events.

We presented here the first large statistical study of extreme geomagnetic storms ever conducted. It provides detailed information on the most intense storms during 1868–2010. Based on this, we identified some key characteristics of extreme storms. The study highlights the importance of the often complex structure of the sources in the solar wind. These findings provide important information for the direction of future space weather forecasting efforts. The comprehensive set of intense storm parameters provided here also forms a useful basis for future studies of exceptional events.

Acknowledgements The results presented in this article use several data sets kindly provided by the listed contributors: The Dcx index was provided by the University of Oulu, Finland, at <http://dcx.oulu.fi>. The Kp index was provided GeoForschungs Zentrum (GFZ) in Potsdam. The geomagnetic observatory hourly values were obtained from the WDCC1 for Geomagnetism in Edinburgh, which in turn obtained the data from the world-wide network of magnetometers. The OMNI data were provided from the GSFC/SPDF OMNI-Web interface at <http://omniweb.gsfc.nasa.gov>. The SSC lists were obtained from the International Service of Geomagnetic Indices (ISGI) and the National Geophysical Data Center (NGDC). The GLE-event data was provided by the NMDB project (www.nmdb.eu), which in turn obtained the data from the world-wide network of neutron monitors.

The work has received funding from the European Union Seventh Framework Programme (FP7/2007–2013) under grant agreement n. 263252 [COMESSEP]. ESP figures are based on the ESA SEPTEM reference proton dataset and software developed under the COMESSEP project. M. Dumbović and B. Vršnak furthermore acknowledge financial support by the Croatian Science Foundation under the project 6212 “Solar and Stellar Variability”.

Any opinion, findings, and conclusions or recommendations expressed in this material are those of the author(s) and do not necessarily reflect the views of the National Science Foundation.

References

- Akasofu, S.-I.: 1981, Energy coupling between the solar wind and the magnetosphere. *Space Sci. Rev.* **28**, 121.
- Araki, T., Funato, K., Igucchi, T., Kamei, T.: 1993, Direct detection of solar wind magnetic pressure effect on ground magnetic field. *Geophys. Res. Lett.* **20**, 775.
- Bartels, J.: 1932, Terrestrial-magnetic activity and its relation to solar phenomena. *Terr. Magn. Atmos. Electr.* **37**, 1.

- Bell, J.T., Gussenhoven, M.S., Mullen, E.G.: 1997, Super storms. *J. Geophys. Res.* **102**(A7), 14189.
- Beeck, J., Sanderson, T.R.: 1989, Mean free path of low-energy protons upstream of selected interplanetary shocks. *J. Geophys. Res.* **94**, 8769.
- Bohlin, J.D.: 1977, Extreme-ultraviolet observations of coronal holes. *Solar Phys.* **51**, 377.
- Bryant, D.A., Cline, T.L., Desai, U.D., McDonald, F.B.: 1962, Explorer 12 observations of solar cosmic rays and energetic storm particles after the solar flare of September 28, 1961. *J. Geophys. Res.* **67**, 4983.
- Burton, R.K., McPherron, R.L., Russell, C.T.: 1975, An empirical relationship between interplanetary conditions and Dst. *J. Geophys. Res.* **80**, 4204.
- Cane, H.V.: 1985, The evolution of interplanetary shocks. *J. Geophys. Res.* **90**, 191.
- Cane, H.V.: 1988, The large-scale structure of flare associated interplanetary shocks. *J. Geophys. Res.* **93**, 1.
- Cane, H.V.: 2000, Coronal mass ejections and Forbush decreases. *Space Sci. Rev.* **93**(1/2), 55.
- Cane, H.V., Richardson, I.G.: 2003, Interplanetary coronal mass ejections in the near-Earth solar wind during 1996–2002. *J. Geophys. Res.* **108**, A4. DOI.
- Cane, H.V., Richardson, I.G., Roseninge, T.T.: 1996, Cosmic ray decreases: 1964–1994. *J. Geophys. Res.* **101**, 21561. DOI.
- Cane, H.V., Richardson, I.G., Roseninge, T.T.: 2010, A study of solar energetic particle events of 1997–2006: their composition and associations. *J. Geophys. Res.* **115**, 8101.
- Chilingarian, A., Bostanjyan, N.: 2010, On the relation of the Forbush decreases detected by ASEC monitors during the 23rd solar activity cycle with ICME parameters. *Adv. Space Res.* **45**, 614.
- Cliver, E.W., Ling, A.G., Wise, J.E., Lanzerotti, L.J.: 1999, A prediction of geomagnetic activity for solar cycle 23. *J. Geophys. Res.* **104**, 6871.
- Cliver, E.W., Kamide, Y., Ling, A.G.: 2002, The semiannual variation of geomagnetic activity: phases and profiles for 130 years. *J. Atmos. Solar-Terr. Phys.* **64**, 47.
- Cohen, C.M.S.: 2006, Observations of energetic storm particles: an overview, solar eruptions and energetic particles. In: Gopalswamy, N., Mewaldt, R., Torsti, J. (eds.) *Solar Eruptions and Energetic Particles, Geophysical Monograph Series* **165**, 275.
- Cooke, D.J., Humble, J.E., Shea, M.A., Smart, D.F., Lund, N.: 1991, On cosmic-ray cut-off terminology. *Nuovo Cimento C* **14**, 213.
- Cortie, A.L.: 1912, Sunspots and terrestrial magnetic phenomena 1898–1911: the cause of the annual variation in magnetic disturbances. *Mon. Not. Roy. Astron. Soc.* **73**, 52.
- Crooker, N.U., Feynman, J., Gosling, J.T.: 1977, On the high correlation between long-term averages of solar wind speed and geomagnetic activity. *J. Geophys. Res.* **82**, 1933.
- Crooker, N.U., Cliver, E.W., Tsurutani, B.T.: 1992, The semiannual variation of great geomagnetic storms and the post-shock Russell–McPherron effect preceding coronal mass ejecta. *Geophys. Res. Lett.* **19**, 429.
- Crosby, N.B., Heynderickx, D., Jiggins, P., Aran, A., Sanahuja, B., Truscott, P., Lei, F., Jacobs, J., Poedts, S., Gabriel, S., Sandberg, I., Glover, A., Hilgers, A.: 2015, SEPEM: a tool for statistical modelling the solar energetic particle environment. *Space Weather* **13**. DOI.
- Dungey, J.R.: 1961, Interplanetary magnetic fields and auroral zones. *Phys. Rev. Lett.* **6**, 47.
- Dierckx, M., Tziotziou, K., Dalla, S., Patsou, I., Marsh, M.S., Crosby, N.B., Malandraki, O., Tsiropoula, G.: 2015, Relationship between solar energetic particles and properties of flares and CMEs: statistical analysis of solar cycle 23 events. *Solar Phys.* **290**(3), 841. DOI.
- Dumbović, M., Vršnak, B., Čalogović, J., Karlica, M.: 2011, Cosmic ray modulation by solar wind disturbances. *Astron. Astrophys.* **531**, A91. DOI.
- Dumbović, M., Vršnak, B., Čalogović, J., Župan, R.: 2012, Cosmic ray modulation by different types of solar wind disturbances. *Astron. Astrophys.* **538**, A28. DOI.
- Echer, E., Gonzales, W.D., Tsurutani, B.T.: 2008, Interplanetary conditions leading to superintense geomagnetic storms (Dst < −250 nT) during solar cycle 23. *Geophys. Res. Lett.* **35**, L06S03. DOI.
- Feldstein, Y.I., Grafe, A., Gromova, L.I., Popov, V.A.: 1997, Auroral electrojets during geomagnetic storms. *J. Geophys. Res.* **102**, 14223.
- Feynman, J., Crooker, N.U.: 1978, The solar wind at the turn of the century. *Nature* **275**, 626.
- Forbush, S.E.: 1937, On the effects in cosmic-ray intensity observed during the recent magnetic storm. *Phys. Rev.* **51**, 1108.
- Gonzalez, A.L.C., Gonzales, W.D., Dutra, S.L.G., Tsurutani, B.T.: 1993, Periodic variations in geomagnetic activity: a study based on the Ap index. *J. Geophys. Res.* **98**, 9215.
- Gonzalez, W.D., Joselyn, J.A., Kamide, Y., Kroehl, H.W., Rostoker, G., Tsurutani, B.T., Vasyliunas, V.M.: 1994, What is a geomagnetic storm? *J. Geophys. Res.* **99**, 5771.
- Gonzalez, W.D., Tsurutani, B.T., Lepping, R.P., Schwenn, R.: 2002, Interplanetary phenomena associated with very intense geomagnetic storms. *J. Atmos. Solar-Terr. Phys.* **64**, 173.
- Gonzalez, W.D., Echer, E., Clua-Gonzalez, A.L., Tsurutani, B.: 2007, Interplanetary origin of intense geomagnetic storms (Dst < −100 nT) during solar cycle 23. *Geophys. Res. Lett.* **34**, L06101. DOI.

- Gonzalez, W.D., Echer, E., Tsurutani, B.T., Gonzales, A., Dal Lago, A.: 2011a, Interplanetary origin of intense, superintense and extreme geomagnetic storms. *Space Sci. Rev.* **158**, 69.
- Gonzalez, W.D., Echer, E., Clua de Gonzales, A.L., Tsurutani, B.T., Lakhina, G.S.: 2011b, Extreme geomagnetic storms, recent Gleissberg cycles and space era – superintense storms. *J. Atmos. Solar-Terr. Phys.* **73**, 1447.
- Gosling, J.T., Bame, S.J., McComas, D.J., Phillips, J.L.: 1990, Coronal mass ejections and large geomagnetic storms. *Geophys. Res. Lett.* **17**, 901.
- Huttunen-Heikinmäki, K., Valtonen, E.: 2009, Interplanetary fast forward shocks and energetic storm particle events above 1.5 MeV. *Ann. Geophys.* **27**, 767.
- Kallenrode, M.-B.: 1995, Particle acceleration at interplanetary shocks – observations at a few tens of keV some tens of MeV. *Adv. Space Res.* **15**(8–9), 375.
- Kamide, Y., Yokoyama, N., Gonzalez, W., Tsurutani, B.T., Daglis, I.A., Brekke, A., Masuda, S.: 1998, Two step development of geomagnetic storms. *J. Geophys. Res.* **103**, 6917.
- Kan, J.R., Lee, L.C.: 1979, Energy coupling and the solar wind dynamo. *Geophys. Res. Lett.* **6**, 577.
- Karinen, A., Mursula, K.: 2005, A new reconstruction of the Dst index for 1932–2002. *Ann. Geophys.* **23**, 475.
- Klecker, B., Scholer, M., Hovestadt, D., Gloeckler, G., Ipavich, F.M.: 1981, Spectral and compositional variations of low energy ions during an energetic storm particle event. *Astrophys. J.* **251**, 393.
- Lee, M.A.: 2005, Coupled hydromagnetic wave excitation and ion acceleration at an evolving coronal/interplanetary shock. *Astrophys. J. Suppl.* **158**, 38.
- Léfevre, L., Vennerström, S., Dumbović, M., Vršnak, B., Sudar, D., Arltl, R., Clette, F., Crosby, N.: 2016, Detailed analysis of solar data related to historical extreme geomagnetic storms: 1868–2010. *Solar Phys.* In this issue. DOI.
- Legrand, J.P., Simon, P.A.: 1981, Ten cycles of solar and geomagnetic activity. *Solar Phys.* **70**, 173.
- Lockwood, M., Rouillard, A.P., Finch, I.D.: 2009, The rise and fall of open solar flux during the current grand solar maximum. *Astrophys. J.* **700**, 937.
- Mäkelä, P., Gopalswamy, N., Akiyama, S., Xie, H., Yashiro, S.: 2011, Energetic storm particle events in coronal mass ejection-driven shocks. *J. Geophys. Res.* **116**, A08101. DOI.
- Malandraki, O.E., Lario, D., Lanzerotti, L.J., Sarris, E.T., Geranos, A., Tsiropoula, G.: 2005, October/November 2003 ICMEs: ACE/EPAM solar energetic particle observations (Special Section: ‘Violent Sun – Earth Connection Events of October–November 2003’). *J. Geophys. Res.* **110**, A09S06. DOI.
- Mayaud, P.N.: 1973, *A 100-Year Series of Geomagnetic Data: Indices Aa, Storm Sudden Commencements*, IAGA Bull. **33**, Internat. Union of Geod. and Geophys., Paris.
- McIntosh, D.H.: 1959, On the annual variation of magnetic disturbance. *Phil. Trans. Roy. Soc. London Ser. A, Math. Phys. Sci.* **251**, 525.
- Meng, C.-I.: 1984, Dynamic variation of the auroral oval during intense magnetic storms. *J. Geophys. Res.* **89**, 227.
- Milan, S.E., Boakes, P.D., Hubert, B.: 2008, Response of the expanding/contracting polar cap to weak and strong solar wind driving: implications for substorm onset. *J. Geophys. Res.* **113**, A09215. DOI.
- Milan, S.E., Hutchinson, J., Boakes, P.D., Hubert, B.: 2009, *Ann. Geophys.* **27**, 2913.
- Mursula, K., Holappa, L., Karinen, A.: 2008, Correct normalization of the Dst index. *Astrophys. Space Sci. Trans.* **4**, 41.
- Nakai, H., Kamide, Y.: 2003, Substorm-associated large-scale magnetic field changes in the magnetotail: a prerequisite for “magnetotail deflation” events. *Ann. Geophys.* **21**, 869.
- van Nes, P., Roelof, E.C., Reinhard, R.: 1984a, Diffusion coefficients of low energy protons upstream of quasi-parallel interplanetary shocks. *Adv. Space Res.* **4**, 315.
- van Nes, P., Reinhard, R., Sanderson, T.R., Wenzel, K.-P., Zwickl, R.D.: 1984b, The energy spectrum of 35- to 1600-keV protons associated with interplanetary shocks. *J. Geophys. Res.* **89**, 2122.
- Nevanlinna, H., Kataja, E.: 1993, An extension of the geomagnetic activity index series aa for two solar (1844–1868). *Geophys. Res. Lett.* **20**, 2703.
- Newell, P.T., Sotirelis, T., Liou, K., Meng, C.-I., Rich, F.J.: 2007, A nearly universal solar wind-magnetosphere coupling function inferred from 10 magnetospheric state variables. *J. Geophys. Res.* **112**, A01206. DOI.
- Newton, H.W.: 1948, A distinctive geomagnetic epoch, 1941 June 9–14. *Observatory* **68**, 60.
- Reames, D.V.: 1999, Particle acceleration at the Sun and in the heliosphere. *Space Sci. Rev.* **90**, 413.
- Richardson, I.G., Cane, H.V.: 2010, Near-Earth interplanetary coronal mass ejections during solar cycle 23 (1996–2009): catalog and summary of properties. *Solar Phys.* **264**, 189. DOI.
- Richardson, I.G., Cane, H.V.: 2011a, Galactic cosmic ray intensity response to interplanetary coronal mass ejections/magnetic clouds in 1995–2009. *Solar Phys.* **270**, 609.
- Richardson, I.G., Cane, H.V.: 2011b, Geoeffectiveness (Dst and Kp) of interplanetary coronal mass ejections during 1995–2009 and implications for storm forecasting. *Space Weather* **9**, S07005. DOI.

- Richardson, I.G., Webb, D.F., Zhang, J., Berdichevsky, D.B., Biesecker, D.A., Kasper, J.C., Kataoka, R., Steinberg, J.T., Thompson, B.J., Wu, C.-C., Zhukov, N.: 2006, Major geomagnetic storms ($Dst \leq 100$ nT) generated by co-rotating interaction regions. *J. Geophys. Res.* **11**, A07S09. DOI.
- Russell, C.T., McPherron, R.L.: 1973, Semiannual variation of geomagnetic activity. *J. Geophys. Res.* **78**, 92.
- Sarris, E.T., van Allen, J.: 1974, Effects of interplanetary shock waves on energetic charged particles. *J. Geophys. Res.* **79**, 4157.
- Siscoe, G.L., Formisano, V., Lazarus, A.J.: 1968, Relation between geomagnetic sudden impulses and solar wind pressure changes – an empirical investigation. *J. Geophys. Res.* **73**, 4869.
- Skoug, R.M., Gosling, J.T., Steinberg, J.T., McComas, D.J., Smith, C.W., Ness, N.F., Hu, Q., Burlaga, L.F.: 2004, Extremely high speed solar wind: 29–30 October 2003. *J. Geophys. Res.* **109**, A09102. DOI.
- Smart, D.F., Shea, M.A., Flückiger, E.O.: 2000, *Space Sci. Rev.* **93**, 305.
- Sugiura, M.: 1964, Hourly values of equatorial Dst for the IGY. *Ann. Int. Geophys. Year* **35**, 49.
- Svalgaard, L.: 1977, Geomagnetic activity: dependence on solar wind parameters. In: Zirker, J.B. (ed.) *Coronal Holes and High Speed Wind Streams*, Colorado Associated University Press, Boulder, 371.
- Svalgaard, L., Cliver, E.W., Ling, A.G.: 2002, The semiannual variation of great geomagnetic storms. *Geophys. Res. Lett.* **29**, 1765.
- Svalgaard, L., Cliver, E.W.: 2010, Heliospheric magnetic field 1835–2009. *J. Geophys. Res.* **115**. DOI.
- Tsurutani, B.T., Lakhina, G.S.: 2013, An extreme coronal mass ejection and consequences for the magnetosphere and Earth. *Geophys. Res. Lett.* DOI.
- Tsurutani, T., Lakhina, G.S.: 2014, An extreme coronal mass ejection and consequences for the magnetosphere and Earth. *Geophys. Res. Lett.* **41**, 287.
- Tsurutani, B.T., Gonzales, W.D., Tang, F., Lee, Y.T.: 1992, Great magnetic storms. *Geophys. Res. Lett.* **19**, 73.
- Tsurutani, B.T., Echer, E., Guarnieri, F.L., Koyzera, J.U.: 2008, CAUSES November 7–8, 2004, superstorm: complex solar and interplanetary features in the post-solar maximum phase. *Geophys. Res. Lett.* **35**, L06S05. DOI.
- Vennerstroem, S.: 2000, Long-term rise in geomagnetic activity – a close connection between quiet days and storms. *Geophys. Res. Lett.* **27**, 69.
- Vennerstroem, S.: 2001, Interplanetary sources of magnetic storms: a statistical study. *J. Geophys. Res.* **106**, 29175.
- Verbanac, G., Živković, S., Vršnak, B., Bandić, M., Hojsak, T.: 2013, Comparison of geoeffectiveness of coronal mass ejections and corotating interaction regions. *Astron. Astrophys.* **558**, A58.
- Wang, Y.M., Ye, P.Z., Wang, S., Xue, X.H.: 2003, An interplanetary cause of large geomagnetic storms: fast forward shock overtaking preceding magnetic cloud. *Geophys. Res. Lett.* **30**(13), 1700.
- Wu, C.-C., Dryer, M.: 1996, Predicting the initial IMF Bz polarity's change at 1 AU caused by shocks that precede coronal mass ejections. *Geophys. Res. Lett.* **23**, 1709.
- Zhang, J., Richardson, I.G., Webb, D.F.: 2008, Interplanetary origin of multi-dip geomagnetic storms. *J. Geophys. Res.* **113**, A00A12. DOI.
- Zhang, J., Richardson, I.G., Webb, D.F., Gopalswamy, N., Huttunen, E., Kasper, J.C., Nitta, N.V., Poomvises, W., Thompson, B.J., Wu, C.-C., Yashiro, S., Zhukov, A.N.: 2007, Solar and interplanetary sources of major geomagnetic storms ($Dst < -100$ nT) during 1996–2005. *J. Geophys. Res.* **112**, A10102. DOI.
- Zurbuchen, T.H., Gloeckler, G., Ipavich, F., Raines, J., Smith, C.W., Fisk, L.A.: 2004, On the fast coronal mass ejections in October/November 2003: ACE-SWICS results. *Geophys. Res. Lett.* **31**, L11805. DOI.